



SRI KRISHNA COLLEGE OF TECHNOLOGY

[An Autonomous Institution | Affiliated to Anna University and Approved by
AICTE | Accredited by NAAC – UGC with 'A' Grade]

KOVAIPUDUR, COIMBATORE – 641042,INDIA



info@skct.edu.in | www.skct.edu.in

Ph:+91 422 2604567 to 70 | Fax: +91 422 2607152

CRITERIA 3

3.7.1 – Collaborative Activities

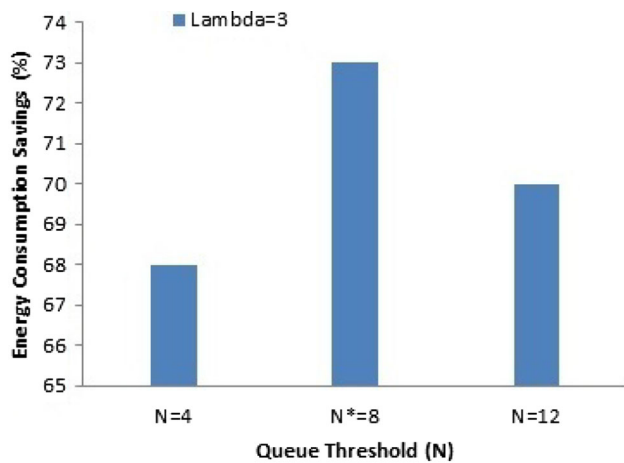


Fig. 10 Case (a)—queue threshold (N) versus energy consumption savings (%)

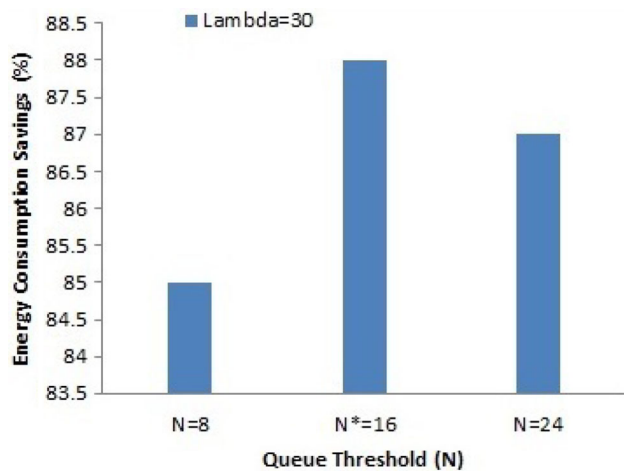


Fig. 11 Case (b)—queue threshold (N) versus energy consumption savings (%)

Table 4 Performance measures at N^* of CM and CH

Role of sensor node	Performance measures at N^*	
	Mean delay (m sec)	Energy consumption savings (%)
CM	1167	73
CH	262	88

cases. The trade-off that exist between the mean delay and the average energy consumption is clearly explored trough the obtained results when the sensor node act as CM and CH.

From the Table 4, it is inferred that the maximum energy saving (%) is obtained when the sensor node acts as CH when compared to that of node acting as CM at optimal threshold. It is also found that the mean delay is less when the sensor node acts as CH when compared to that of node acting as CM at optimal threshold.

6 Conclusions and future work

This paper proposes an energy minimization technique using N-policy $M/M/1$ queueing model of a sensor node in a cluster acting as Cluster Member (CM) and Cluster Head (CH) which prolongs the lifetime of the network. An analytical model of a cluster based sensor network using N-policy $M/M/1$ queueing model is developed and the performance of the proposed model is analysed in terms of average energy consumption and mean delay when the node acts as CM and CH. The expression for the optimal value of threshold (N^*) for which the node consumes minimum energy is also derived analytically. Results show that the average energy consumption savings is high when the node acts as CH when compared to node acting as CM and the trade-off exist between the average energy consumption and mean delay is also explored. Simulations are performed and the results obtained show that the simulation results match with the analytical results thus validating the accuracy of the approach. The buffer capacity is assumed to be infinite for the sake of approximation and channel contention is assumed to be free but in reality, the buffer capacity is finite and contention between the nodes exists. Hence, the performance analysis of a node by considering finite buffer capacity and the channel contention will be another interesting area of future research.

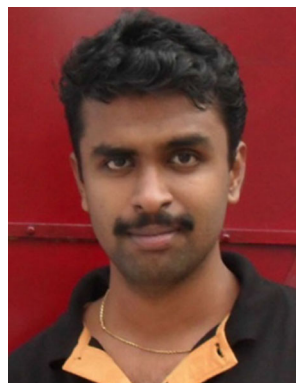
References

1. Quan, Z., Subramanian, A., Sayed, A.H.: REACA: an efficient protocol architecture for large scale sensor networks. *IEEE Trans. Wirel. Commun.* **6**(10), 3846–3855 (2007)
2. Carle, J., Simplot-Ryl, D.: Energy-efficient area monitoring for sensor networks. *IEEE Comput.* **37**(2), 40–46 (2004)
3. Chiasserini, C.F., Garetto, M.: An analytical model for wireless sensor networks with sleeping nodes. *IEEE Trans. Mob. Comput.* **5**(12), 1706–1718 (2006)
4. Huang, J., Hong, Y., Zhao, Z., Yuan, Y.: An energy-efficient multi-hop routing protocol based on grid clustering for wireless sensor networks. *Clust. Comput.* **20**(4), 3071–3083 (2017)
5. Girod, L., Stathopoulos, T., Ramanathan, N., Elson, J., Estrin, D., Osterweil, E., Schoellhammer, T.: A system for simulation, emulation, and deployment of heterogeneous sensor networks. In: *Proceedings of the 2nd international conference on Embedded networked sensor systems—SenSys '04*, pp. 201–201 (2004)
6. Mhatre, V., Rosenberg, C.P., Kofman, D., et al.: A minimum cost heterogeneous sensor network with a lifetime constraint. *IEEE Trans. Mob. Comput.* **1**(1), 4–15 (2005)
7. Duarte-Melo, E., Liu, M.: Analysis of energy consumption and lifetime of heterogeneous wireless sensor networks. In: *Proceedings of the IEEE Globecom*, pp. 21–25, (2002)
8. Du, X., Xiao, Y.: Energy efficient chessboard clustering and routing in heterogeneous sensor networks. *Int. J. Wirel. Mob. Comput.* **1**(2), 121–130 (2006)
9. Du, X., Lin, F.: Maintaining differentiated coverage in heterogeneous sensor networks. *EURASIP J. Wirel. Comm. Netw.* **2005**(4), 565–572 (2005)

10. Yarvis, M., kushalnagar, N., Singh, H. et al.: Exploiting heterogeneity in sensor networks. In: Proceedings of the IEEE INFOCOM, pp. 878–890 (2005)
11. Xiaojiang, D., Guizani, M., Xiao, Y., Chen, H.-H.: Two tier secure routing protocol for heterogeneous sensor networks. *IEEE Trans. Wirel. Commun.* **6**(9), 3395–3401 (2007)
12. Jayaparvathy, R., Maheswar, R.: Energy minimization scheme for cluster based sensor networks. *Int. J. Recent Trends Eng. Technol.* **6**(2), 164 (2009)
13. Jiang, F.C., Huang, D.C., Yang, C.T., Leu, F.Y.: Lifetime elongation for wireless sensor network using queue-based approaches. *J. Supercomput.* **59**(3), 1312–1335 (2012)
14. Maheswar, R.: Performance analysis of an energy optimization scheme for cluster based heterogeneous sensor networks. Anna University Thesis, (2012)
15. Maheswar, R., Jayaparvathy, R.: Performance analysis using contention based queueing model for wireless sensor networks. In: Proceedings of the International Congress for global, Science and Technology, pp. 59–59, (2010)
16. Maheswar, R., Jayaparvathy, R.: Performance analysis of cluster based sensor networks using N-Policy M/G/1 queueing model. *Eur. J. Sci. Res.* **58**(2), 177–188 (2011)
17. Maheswar, R., Jayaparvathy, R.: Performance analysis of fault tolerant node in wireless sensor network. In: Proceedings of the Third International Conference on Advances in Communication, Network, and Computing, CNC 2012, Chennai, India, February 24–25, (2012)
18. Rasouli, R., Ahmadi, M.: Energy consumption estimation in clustered wireless sensor networks using M/M/1 queueing model. *Int. J. Wirel. Mob. Netw.* **5**(1), 15 (2013)
19. Maheswar, R., Jayaparvathy, R.: Power control algorithm for wireless sensor networks using N-Policy M/M/1 queueing model. *IJCSE* **2**(7), 2378–2382 (2010)
20. Polastre, J., Hill, J., Culler, D.: versatile low power media access for wireless sensor networks. In: Proceedings of the 2nd International Conference on Embedded Networked Sensor Systems, pp. 95–107, (2004)



R. Maheswar has completed his B.E (ECE) from Madras University in the year 1999, M.E. (Applied Electronics) from Bharathiyar University in the year 2002 and Ph.D. in the field of Wireless Sensor Network from Anna University in the year 2012. He has about 15 years of teaching experience at various levels and presently working as a Professor in the Electronics and Communication Engineering Department, Sri Krishna College of Technology, Coimbatore. He has published 35 papers at International Journals and International Conferences. His research interest includes Wireless Sensor Network, Queueing theory and Performance Evaluation.



Wireless Network and IoT.

G. R. Kanagachidambaresan received his Bachelor degree in Electrical and Electronics Engineering in 2010, Master's degree in Pervasive Computing Technologies in 2012 and Ph.D. in Information and Communication Engineering in 2017. He is currently an Associate Professor in Department of Computer Science and Engineering in Veltech Rangarajan Dr.Sagunthala R&D Institute of Science and Technology. His main research interest includes Body Sensor Network, Fault tolerant



D. Nageswari has completed her B.E (ECE) from Anna University in the year 2010, M.E (Applied Electronics) from Anna University in the year 2014. She has about 7 years of teaching experience and presently working as an Assistant Professor in the Electronics and Communication Engineering Department, Sri Krishna College of Technology, Coimbatore. Her area of research interest is Wireless Sensor Network.

Survey on Similar Object Detection in H.264 Compressed Video

K.Srinivasan

Assistant Professor

Department of Electronics and
Communication Engineering

Sri Krishna College of Technology,
Coimbatore.

seenu84@gmail.com

P.Balamurugan

Principal/Professor

Department of Electrical and
Electronics Engineering

Mount Zion College of Engineering
& Technology, Pudukkottai

V.R.Azhaguramyaa

Assistant Professor

Department of Computer Science
and Engineering

Sri Krishna College of Engineering
& Technology, Coimbatore

Abstract: *Similar object detection is an important feature that must be included in any object tracking application which will have great impact on video surveillance. Object tracking is a dynamic optimization process based on the temporal information related to the previous frames. The primary steps of object tracking are preprocessing, background subtraction and segmentation, similar object detection and object tracking. Self-similarity [23] is an attractive image property which has recently found its way into object recognition in the form of local self-similarity descriptors. In this work, global as well as local self-similarity descriptors are discussed to find the similar object detection.*

Keywords: *Similar object detection, local self-similarity descriptor, Global self-similarity descriptor*

I INTRODUCTION

Object tracking assumes a basic part in PC vision with wide usages in video observation, human PC cooperation, vehicle route, and so on. Given the target object at the main edge, the objective of tracking is to find this object for the ensuing casings [1]. Ongoing object tracking is a standout amongst essential prerequisites for independent portable robots. Vision-oriented object tracking needs chose focuses to be tracked and comparing focuses to be looked in every casing [2]. At first video, occasion detection needs detecting and tracking objects initially, and after that perceiving what is going on around those tracked objects [3]. Target objects can be characterized by their appearances, for example, shading, surface, edges, and shape data, which give trademark data about the object. This trademark data, assembled from a format or an arrangement of layouts of the target object, is encoded into a cost or comparability work. Tracking algorithms then decide the correspondence of the object area in back to back pictures by advancing the pre-decided comparability utilitarian [4]. There are different techniques utilized for object detection and tracking. Objects are regularly detected by utilizing point detector systems (e.g., as SIFT), background subtraction, division (e.g., as diagram cut or dynamic shapes), or learning components (e.g., as Adaboost or SVM) [5].

Such methods included the constant use of a detection algorithm in individual edges and the relationship of the detections crosswise over edges [6]. A post-processing task refines the detection by evaluating and fitting an arrangement of ovals that characterize the motion of the object to the past arrangement of moving locales [7]. After object detection, its tracking is done. A successful tracker ought to handle the varieties both of the objective and the foundation well. In the meantime, the proficiency of the tracker ought to likewise be measured [8]. The level set technique is one such capable instrument for object tracking in picture successions because of its adaptability with reference to topological variations of the shapes [9]. And additionally, the particle filter oriented tracker is an inspecting oriented tracking technique, which can adapt well to the non-direct and non-Gaussian tracking issues [10]. In these days division oriented tracking have pulled in incredible consideration in the field of object tracking. It could give a more exact frontal area/foundation partition, contrasted with established tracking techniques which frequently utilize a bouncing box to characterize the objective question. This is especially critical for tracking non-unbending objects, for example, hands and people on foot since division would present less undesirable foundation data and support the floating issue in a specific degree [11].

Despite the fact that similarly object detection and tracking is done utilizing different apparatus, however, fruitful movement detection in real duration usage is a troublesome undertaking on account of such a variety of difficulties which incorporate brightening variations, fake movement, Gaussian commotion out of sight and so on that may prompt improper movement detection [12]. And also tracking the deformable object in reasonable situations is still challenging in light of the fact that the objective appearance may vary continually amid moving, particularly for an unpredictable molded object, difficulties mostly originate from the characteristic varieties, for example, mutilation, turn and scaling [13]. These may bring about confuse or lose object amid tracking and lessen the precision of tracker. To take care of these issues, researchers have proposed a

considerable measure of algorithms which can be isolated into two classes, one is a discriminative strategy; the other is generative technique [14]. Further to solve those difficulties, most top-performing techniques depend on web-based learning-based algorithms to adaptively upgrade target appearance. In these strategies, visual tracking is planned as an online twofold characterization issue and the objective appearance designs are overhauled adaptively utilizing the pictures tracked from the past casings [15]. These strategies could be favored for object detection and tracking.

II LITERATURE SURVEY

Most object tracking strategies connected in the video reconnaissance field depend on the earlier pattern acknowledgment of the moving items. These strategies are not sufficient for tracking various objects in the meantime on the grounds that the pattern of each moving object ought to be earlier mentioned. Mohamed Jedra, *et al.* [16] acquainted another technique to conquer that issue. Without a doubt, another ongoing methodology was built up in view of the molecule channel and foundation subtraction. That approach could identify and track consequently, different moving objects with no learning stage or earlier information about the size, nature or the underlying location. An exploratory study was performed among few video test sets. The acquired yields demonstrated that the new technique could effectively handle numerous unpredictable circumstances. An examination of different techniques informed that the proposed approach was more worthwhile in detecting objects and also tracking them.

DorraRahia and Guillaume-Alexandre Bilodeau, [17] exhibited a powerful online multiple objects tracking (MOT) method in view of different elements. Their approach could deal with MOT issues, such as long haul and substantial impediments and close comparability between aimed appearance designs. The proposed MOT algorithm depended on the idea of the multi-highlight combination. It chose the best location of the tracked focus by utilizing a vigorous appearance display representation. The appearance model of an objective was worked with a shading model, a meager appearance demonstrates, a movement show and a spatial data display. With a specific end goal to choose the ideal applicant (discovery reaction) of the objective, they ascertained a straight proclivity work that coordinated likeness scores originating from every component. They detailed the issue as an information affiliation issue between an arrangement of detections and an arrangement of focuses as per their joint likelihood values. The proposed strategy had been assessed on open video

arrangements. From above discussion, they exhibited that their MOT system accomplished aggressive results and was fitted for taking care of a few testing issues.

Hainan Zhao, *et al.* [18] broadened sparse representation based classification (SRC) and multi-feature hashing (MFH) into various object tracking assignment and proposed a joint appearance model of SRC and MFH, which went for separating distinctive objects viably. Not at all like most past methodologies which just concentrated on creating appearance models for all objectives, had we additionally concentrated on discriminative elements for recognizing troublesome sets of targets. Firstly, an SRC based worldwide discriminative appearance model was intended for separating all objectives. That planned tracks relationship as an SRC issue. A discriminative word reference learning methodology was presented, which enhanced the SRC characterization execution. Along these lines, the worldwide discriminative appearance model could recognize various targets all the more viably. Besides, an MFH oriented pairwise appearance model was planned. That pairwise appearance demonstrates concentrated on discernable components from two focuses without focusing on different targets or foundations, hence that was more compelling for separating particular close-by tracks sets. Information affiliation structure was utilized to produce last tracks. Significant execution changes were appeared on testing information sets, especially in measurements of personality switches.

Small dim target tracking is a dynamic and imperative research territory in picture preparing and pattern acknowledgment. As of late, there has been an accentuation on the advancement of algorithms in light of spatial area Constant False Alarm Rate (CFAR) location. Ahmadi, *et al.* [19] showed a novel algorithm for detecting and tracking little diminish focused in Infrared (IR) picture arrangements with low Signal to Noise Ratio (SNR) in light of the frequency and spatial area data. Utilizing a Dual-Tree Complex Wavelet Transform (DT-CWT), a CFAR detector was connected in the frequency space to discover potential places of items in a casing. Taking after that progression, a Support Vector Machine (SVM) arrangement was connected to acknowledge or dismiss every potential point in light of the spatial space data of the edge. The blend of the frequency and spatial area data showed the high effectiveness and precision of the proposed strategy which was upheld by the trial comes about.

Zheng, *et al.* [20] displayed a structure for tracking multiple objects imaged from at least one static camera, where the issues of object detection and data association were communicated by a solitary target work. Especially, they consolidated a

sparsity-driven detector with the system stream information affiliation method. The system took after the Lagrange double decay technique, exploiting the usage of frequently corresponding nature of the two dual issues. Their coupling plan kept away the issue of mistake spread from which customary "detection-tracking methodologies" to various object tracking endured. They likewise shunned basic heuristics, for example, "non-greatest concealment" of theories by displaying the joint picture probability rather than applying free probability presumptions. Their coupling algorithm was ensured to join and could overcome the defects in track upkeep because of regular impediment and unclear appearance between items. Besides, their strategy did not have extreme versatility problems but rather could handle many edges in the meantime. Their tests included testing, remarkably unmistakable datasets and exhibited that their technique could accomplish comes about practically identical to or superior to those of state-of-art methodologies.

Object tracking is a dynamic improvement prepared in view of the worldly data identified with the past casings. Proposing a technique with higher accuracy in complex situations is a test for scientists in this field of study. Faegheh, *et al.* [21] proposed an object tracking strategy in light of a meta-heuristic method. Despite the fact that there were few meta-heuristic methodologies in the concept, they had adjusted GbSA (galaxy based search algorithm) which was more exact than related works. The GbSA looked the state space by recreating the development of the winding system to locate the ideal question state. The proposed technique looked every edge of video with molecule channel and the MGSbA in a comparable way. That got a present edge and the worldly data that was identified with past casings as information and tried to locate the ideal object state in every one. The trial comes about demonstrated the proficiency of that algorithm in correlation with aftereffects of related strategies.

Weihao Gan, *et al.* [22] introduced a temporal prediction and spatial refinement (TPSR) technique for online single object tracking (SOT). The TPSR tracking framework comprised of three combined modules: pre-preparing (PP), temporal prediction (TP) and spatial refinement (SR). Enlightenment variety and shaking camera development were two testing variables in the tracking issue. They were initially repaid in the PP module. At that point, a joint locale-oriented template matching (TM) and pixel-wised optical flow (OF) plan was received in the TP module, where the switch amongst TM and OF was led consequently. Those two modes worked in a corresponding way to handle distinctive closer view and foundation circumstances. At long last, to beat the floating blunder emerging from the TP

module, the bounding box area, and size were well tuned utilizing the neighborhood spatial data of the new casing in the SR module. The proposed TPSR tracking framework offered the best in class execution with reference to the regularly utilized benchmarking dataset.

III FEATURES OF SELF-SIMILARITY

Extracting self-similarity information of an image is finding all regions within this image that look alike [23]. A similarity measurement between patches must be defined and a retrieval algorithm on the image must be specified. [Shechtman and Irani, 2007]'s definition of local self-similarity (LSS) on a patch-level forms the basis of computing self-similarities. On this basis, [Deselaers and Ferrari, 2010] designed their global algorithm.

3.1 Local Self-Similarity Feature

Taking the patches around two pixels, we can measure their similarity by calculating the sum of squared distances of their pixel values[23].

Definition 1. SSD. For two pixels p and p_0 of the image I , let t_p and t_{p_0} denote the $w \times w$ patches centered around p respectively p' [23]. The Sum of Squared Distances (SSD) of patch t_p and t_{p_0} is calculated on each pixel value $t_{p,i}$ and $t_{p',i}$ as

$$SSD(t_p, t_{p'}) = \sum_i (t_{p,i} - t_{p',i})^2.$$

A low SSD value between two patches indicates strong similarity. However, the correlation of two patches is depicted by a correlation value between 0 and 1. A high value reflects strong correlation, where the maximum value 1 states equality. The correlation of the two patches is calculated on their SSD value.

Definition 2. Correlation. Let t_p be a patch centered around pixel p and t_x a patch centered around pixel x . The correlation of two t_p and t_x is reflected by a correlation value $C_p(x) \in (0; 1]$. $C_p(x)$ is the negative exponent of normalized sum of squared distances; i.e.,

$$C_p(x) = \exp\left(-\frac{SSD(t_p, t_x)}{\sigma}\right).$$

In the original publication of LSS a pixels patch t_p is compared to each others pixels patch t_x within a larger region R_p around p ; i.e. $x \in R_p$. All correlation values $C_p(x)$ of the region R_p together form a correlation surface C_p , which is of the same size as R_p [23].

Definition 3. Local Self-Similarity Feature. Let p be an arbitrary pixel, t_p the patch centered around p , and R_p a larger region around p . The Local Self-Similarity Feature is the correlation surface C_p of p to each $x \in R_p$.

$$C_p = C_p(x), \forall x \in R_p$$

3.2 Global Self-Similarity Feature

The naive way to calculate global self-similarities is to directly apply the LSS feature to not just to a restricted region R_p around a pixel, but to the whole image I . This yield in total $H \times W$ correlation surfaces C_p , one for each pixel $p \in I$

Definition 1. Direct Global Self-Similarity Feature. The direct global self-similarity tensor S_I of the image I consists of all the correlation surfaces C_p of each pixel p in the image I .

$$S_I(p, p') = C_p(p'), \forall p, p' \in I.$$

Restricting the correlation surface to a small region R_p around pixel p in the LSS features was to maintain feasibility.

Definition 2. Prototype Codebook. Let θ be a prototype patch of size $w \times w$ that defines a image basic pattern. The set Θ which contains all the prototype patches θ , is the codebook of the efficient GSS tensor.

IV CONCLUSION

Similar object detection can be done using any of the two well known techniques ie., global self-similarity descriptor and local self-similarity descriptor. Most of the researchers may prefer Local self-similarity descriptor rather than global self-similarity descriptor because it is very expensive to compute similarity and local self-similarity descriptors can be easily used in machine learning framework. In future, the researchers may utilize improved some other object detection algorithm to achieve maximum performance.

REFERENCES

- [1] Chen, Si, Shaozi Li, Rongrong Ji, Yan Yan and Shunzhi Zhu, "Discriminative local collaborative representation for online object tracking", Elsevier on Knowledge-Based Systems, Vol.100, pp.13-24, 2016.
- [2] Yasukawa, Shinsuke, Hirotsugu Okuno, Kazuo Ishii and Tetsuya Yagi, "Real-time object tracking based on scale-invariant features employing bio-inspired hardware", Elsevier on Neural Networks, Vol.81, pp.29-38, 2016.
- [3] Hu, Wu-Chih, Chao-Ho Chen, Tsong-Yi Chen, Deng-Yuan Huang and Zong-Che Wu, "Moving object detection and tracking from video captured by moving camera", Elsevier on Journal of Visual Communication and Image Representation, Vol.30, pp.164-180, 2015.
- [4] Iftikhar Majeed and Omar Arif, "Non-linear eigenspace visual object tracking", Elsevier on Engineering Applications of Artificial Intelligence, Vol.55, pp.363-374, 2016.
- [5] De Gregorio, Massimo, Maurizio Giordano, Silvia Rossi and Mariacarla Staffa, "Experimenting WNN support in object tracking systems", Elsevier on Neurocomputing, Vol.183, pp.79-89, 2016.
- [6] Azab, Maha M., Howida A. Shedeed and Ashraf S. Hussein, "New technique for online object tracking-by-detection in video", Elsevier on IET Image Processing, Vol.8, No.12, pp.794-803, 2014.
- [7] Del-Blanco, Carlos R., Fernando Jaureguizar and Narciso García, "An efficient multiple object detection and tracking framework for automatic counting and video surveillance applications", IEEE Transactions on Consumer Electronics, Vol.58, No.3, pp.857-862, 2012.
- [8] Xin Lia, Qiao Liua, Zhenyu Hea, Hongpeng Wanga, Chunkai Zhanga and Wen-Sheng Chen, "A multi-view model for visual tracking via correlation filters", Elsevier on Knowledge-Based Systems, pp.1-23, 2016.
- [9] Li, Yaochen, Yuanqi Su and Yuehu Liu, "Fast two-cycle curve evolution with narrow perception of background for object tracking and contour refinement", Elsevier on Signal Processing: Image Communication, Vol.44, pp.29-43, 2016.
- [10] Li, Wanyi, Peng Wang and Hong Qiao, "Top-down visual attention integrated particle filter for robust object tracking", Elsevier on Signal Processing: Image Communication, Vol.43, pp.28-41, 2016.
- [11] Cheng, Xuan, Ming Zeng and Xinguo Liu, "Spatially constrained level-set tracking and segmentation of non-rigid objects", Elsevier on Journal of Visual Communication and Image Representation, Vol.38, pp.745-752, 2016.
- [12] Resmi, H. B., V. A. Deepambika and M. Abdul Rahman, "Symmetric Mask Wavelet Based Detection and Tracking of Moving Objects Using Variance Method", Elsevier on Procedia Computer Science, Vol.58, pp. 58-65, 2015.
- [13] Zhuo, Tao, Peng Zhang, Yanning Zhang and Wei Huang, "Deformable object tracking with spatiotemporal segmentation in big vision surveillance", Elsevier in Security, Pattern Analysis, and Cybernetics (SPAC), Elsevier on Neurocomputing, pp. 1-10, 2016.
- [14] Han, Guang, Xingyue Wang, Jixin Liu, Ning Sun, and Cailing Wang, "Robust object tracking based on local region sparse appearance model", Elsevier on Neurocomputing, Vol.184, pp.145-167, 2016.
- [15] Yan Chen, Yingju Shen, Xin Liu and Bineng Zhong, "3D Object Tracking Via Image Sets And Depth-Based Occlusion Detection", Elsevier on Signal Processing, pp.1-8, 2014.

- [16] Elafi, Issam, Mohamed Jedra and Nouredine Zahid, "Unsupervised detection and tracking of moving objects for video surveillance applications", Elsevier on Pattern Recognition Letters, Vol.84, pp.70-77, 2016.
- [17] DorraRiahia and Guillaume-Alexandre Bilodeau, "Online multi-object tracking by detection based on generative appearance models", Elsevier on Computer Vision and Image Understanding, pp.1-41, 2016.
- [18] Hainan Zhao, Shuhan Qi and Xuan Wang, "A joint appearance model of SRC and MFH for multi-objects tracking", Elsevier on Neurocomputing, pp.1-9, 2016.
- [19] Ahmadi, Kaveh and Ezzatollah Salari, "Small dim object tracking using frequency and spatial domain information", Elsevier on Pattern Recognition, Vol.58, pp.227-234, 2016.
- [20] Wu, Zheng and Margrit Betke, "Global optimization for coupled detection and data association in multiple object tracking", Elsevier on Computer Vision and Image Understanding, Vol.143, pp.25-37, 2016.
- [21] Sardari, Faegheh and Mohsen Ebrahimi Moghaddam, "An object tracking method using modified galaxy-based search algorithm", Elsevier on Swarm and Evolutionary Computation, pp.1-12, 2016.
- [22] Weihao Gan, Ming-Sui Lee, Chi-hao Wu and C.-C. Jay Kuo, "Object tracking with temporal prediction and spatial refinement (TPSR)", Elsevier on Signal Processing: Image Communication, Vol.47, pp.303-312, 2016.
- [23] Thomas Deselaers and Vittorio Ferrari, "Global and Efficient Self-Similarity Feature Extractor and Descriptor", Computer Vision and Pattern Recognition (CVPR), 2010.



An energy-aware buffer management (EABM) routing protocol for WSN

P. Jayarajan¹ · G. R. Kanagachidambaresan² · T. V. P. Sundararajan³ · K. Sakthipandi⁴ · R. Maheswar¹ · A. Karthikeyan⁵

© Springer Science+Business Media, LLC, part of Springer Nature 2018

Abstract

Wireless sensor network (WSN) seeks an unequal clustering approach to solve its energy hole and HOTSPOT issue. Increasing the cluster number and decreasing the size of the cluster near the sink equally distribute the load across the network. The approach is to make buffer aware to enhance the network lifetime and avoid data packet drop due to buffer overflow. The increase in buffer size is always not possible in preconfigured sensor nodes, making lifetime and data loss as a major problem. An energy-aware buffer management (EABM) routing protocol is designed to overcome the issue. The memory vacancy and energy level are considered before routing the next hop data to the cluster. The proposed EABM routing protocol is compared with LEACH, LEACH-C, ALEACH and EAR routing protocols to support our claim. The proposed routing protocol provides higher lifetime of 1.17 rounds, 1.1 times throughput and 0.73 times reduced packet drop considering LEACH as a benchmark protocol. The energy and buffer filling near the sink are equally distributed in case of the proposed EABM routing protocol.

Keywords Wireless sensor network (WSN) · Buffer management · Energy efficiency · Energy hole · HOTSPOT

1 Introduction

Continuous, unmanned and a lot of automation concepts are done through wireless sensor network (WSN). The sensor network consists of tiny embedded nodes capable to communicate with each other to attain a single objective. The sensor nodes form clusters and layers to communicate with each other, the layered architecture fits monitoring small region of interest (ROI), whereas the network with vast ROI is monitored

✉ P. Jayarajan
pjayarajan@gmail.com

Extended author information available on the last page of the article

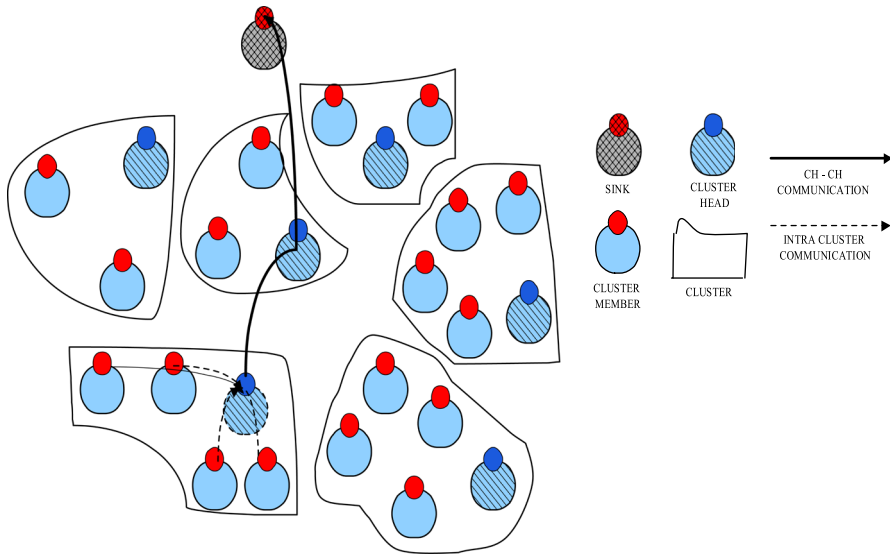


Fig. 1 Clustered WSN architecture

through the clustering approach. The sensor nodes play two major roles (a) cluster member (CM) and (b) cluster head (CH) inside the network like processing and forwarding the data to the sink [1–5]. The selection of CH in the network is done through election methodology considering residual energy, distance as a parameters. The CH aggregates the data from other CM and forwards to the sink for further processing and decision making. The CM senses the event and forwards the data to its CH. The data from the clusters are forwarded to the sink in a multihop fashion [2, 6–10]. The CH maintains table on routing information about the intra-cluster participants, their energy status and its location inside the ROI. The sensor nodes are availed with limited resources like energy, memory and processing capabilities [11–16]. The nodes near the sink face a trouble of losing its energy at a faster rate due to data load from the far away clusters. This is solved through unequal clustering approach creating smaller clusters with fewer participants near the sink. The unequal clustering approach solves energy and HOTSPOT problem [17–22]. This methodology, however, creates drop packets, when the node is with limited buffer capacity and less memory. The data should be forwarded through nodes with high energy and memory capacity [23–29]. Figure 1 illustrates the sensor network clustered architecture clustered approach with sink, CM and CH. The nodes in the sensor network are normally homogenous in nature.

In some occasions, the heterogeneous sensor network comes in action to monitor some applications. In those occasions, the node with superior power and capability takes the role of CH [30–34]. The sensor node becomes energy efficient if it is enabled with the energy harvesting unit such as solar panel and piezoelectric energy harvester. The same node with energy harvesting unit becomes power starving, if the resource to harvest energy becomes zero. The availability of energy is greatly determined by time, place and climatic conditions too. The major monitoring applications are with

homogenous sensor network in which sink alone is powered with permanent power source and high memory capacity. This paper deals with homogenous wireless sensor nodes and organized with related works, proposed routing technique, results and discussion, conclusion and references.

2 Related works

It is understood that energy minimization is a vital issue in the design of systems based on wireless sensor networks. Overall energy minimization in wireless sensor networks can be approached in two ways: network management design and network protocols design [1]. The fundamental idea behind topology control is to build and maintain a reduced topology that will save the small energy budget of sensors while preserving network connectivity and coverage. This can be achieved by reducing the transmission power of sensors. In [2], the authors prove that there is an optimal transmission range that minimizes energy dissipation while keeping a connected topology. WSNs are closely associated with the physical phenomena in their surroundings. The gathered information needs to be associated with the location of the sensor nodes to provide an accurate view of the observed sensor field [1]. Indeed, WSNs may be used for monitoring certain objects for monitoring applications, which also necessitates location information of the sensor nodes being incorporated into the tracking algorithms. Coverage is one of the measurements of WSNs quality of service (QoS), and it is closely related to energy consumption. In some cases, it is possible to obtain energy from external environment (e.g., by using solar cells as power source). There are three different approaches to the problem of conserving energy in WSNs, and all of the approaches must keep the initial coverage QoS. The first approach [16] is to optimize coverage deployment strategy. The second approach is to plan a schedule of active sensors that enables other sensors to go into a sleep mode. The third approach is adjusting the sensing range of sensors for energy conservation. The coverage and connectivity analysis is mainly focused on the issues which are primarily based on the angle of energy consumption, especially in coverage deployment strategy, sleep scheduling mechanism and adjustable coverage radius.

Data mining is an another broad area which contains data preprocessing techniques like data cleaning, data smoothing, data reduction, data compression for improving the network lifetime. Other methods like classification, clustering and association mining mechanism also give attention in data preprocessing. Data-driven approaches can be classified according to problem they addressed. The paper [4] presents an energy aware data acquisition scheme for WSNs that integrates dynamic voltage scaling (DVS) and dynamic modulation scaling (DMS) techniques to minimize the total energy consumption within the networks. Duty cycling techniques [14] are also called as node activity scheduling techniques which reduces the energy consumption of the node. They allow nodes to alternate activity and sleep periods. Indeed, only the sleep state guarantees energy saving since transmitting, receiving and idle listening consumes the scarce and expensive battery power resource. The idea is then to power off the radio subsystem each time it is possible while ensuring an operational network from the application point of view. In [11], the selection of minimum [3] set of active nodes

able to guarantee coverage is based on linear programming techniques. An energy efficient mobility management protocol [12] based on PMIPv6 called sensor proxy mobile IPv6 (SPMIPv6) is proposed. The proposed architecture for SPMIPv6 includes a sensor network-based localized mobility anchor (SLMA), a sensor network-based mobile access gateway (SMAG) and many fully functional IPv6 header stack enabled IP sensor nodes. The simulation results indicate that the proposed scheme reduces the signaling cost as well as the mobility cost against MIPv6 and PMIPv6, showing that the level of energy consumption has been reduced significantly.

Clustering is the activity [13] of creating sets of similar objects. Clustering increases the network scalability and life and cluster heads alone will communicate with cluster head. This reduces the data redundancy which usually happens when each node perform its own data aggregation and transmission [5] function separately. Energy-efficient hierarchical clustering [10] is a probabilistic clustering algorithm and it is an extended version of LEACH with multiple hop architecture. Weight-based clustering [15] is a clustering technique for heterogeneous networks which chooses the better cluster heads thereby increases the lifetime and throughput of WSN.

Geographic and energy aware routing (GEAR) is an energy-efficient routing protocol proposed for routing queries to target regions in a sensor field [17]. In GEAR, the sensors are supposed to have localization hardware equipped, for example, a GPS unit or a localization system so that they know their current positions. Furthermore, the sensors are aware of their residual energy as well as the locations and residual energy of each of their neighbors. GEAR uses energy aware approach that is based on geographic information to select sensors to route a packet toward its destination region. Then, GEAR uses a recursive geographic forwarding algorithm to disseminate the packet inside the target region. Minimum energy communication network (MECN) is a location-based protocol for achieving minimum energy for randomly deployed ad hoc networks, which attempts to set up and maintain a minimum energy network with mobile sensors [18]. It is self-reconfiguring protocol that maintains network connectivity in spite of sensor mobility. It calculates an optimal spanning tree rooted at the sink, called minimum power topology, which contains only the minimum power paths from each sensor to the sink. Small minimum energy communication network (SMECN) is a routing protocol proposed to improve MECN, in which a minimal graph is characterized with regard to the minimum energy property [19]. This property implies that for any pair of sensors in a graph associated with a network, there is a minimum energy-efficient path between them; that is, a path that has the smallest cost in terms of energy consumption over all possible paths between this pair of sensors. Compressive sensing is the technology, where small fragments of signals are reconstructed to form information [35, 36]. This methodology divides the data into smaller fragments and it is forwarded in different paths [37, 38]. The support aided-sparse Bayesian algorithm (SA-SBL) incorporates prior knowledge and learns unknown cluster patterns. The gamma distributions are used for accurate solution attainment.

Increasing the network lifetime by reducing the energy consumption of individual node using queue threshold is an important technique. Here, the packets are buffered until the threshold value is reached and once the threshold value is reached, the packets are transmitted until the queue is empty. The authors in [6–9] discussed the queue threshold model briefly under various scenarios in which they claim that the energy

consumption is highly reduced by reducing the number of transitions between IDLE and BUSY states.

2.1 Energy-aware buffer management

The CH allocation is done through the buffer size and voltage level of the sensor node. The node is considered to be homogenous in nature; hence, all nodes have the same memory size and energy levels. The sensor node accumulates data, aggregates and communicates to the sink. This methodology requires enough memory space when the number of cluster members under the single CH is high. The energy consumed by the node is the factor of distance and the number of bits communicated between the sender and receiver. The omni-directional antenna is realized as a second order radio model as given by Eqs. (1) and (2).

2.2 Radio model

$$E_{trans}(kbits, d) = E_{elec}kbits + E_{fs}kbits d^2; \quad d < d_0$$

$$= E_{elec}kbits + E_{mp}kbits d^4; \quad d > d_0 \tag{1}$$

$$E_{reception}(kbits) = E_{elec}kbits \tag{2}$$

where kbits: no. of bits, d : distance, E_{elec} : energy dissipated per bit to run the transmitter or the receiver circuit, $E_{reception}$: energy dissipated during receiving data, E_{fs} (pJ/(bit-m⁻²)), E_{mp} (pJ/(bit-m⁻²)): energy dissipated per bit to run the transmit amplifier based on the distance between the transmitter and receiver.

The energy consumed by the node exceeds to higher value if the distance between sender and receiver is greater than d_0 (threshold limit). The battery decay process is linear to some extent and exhibits nonlinear property after a particular limit. Table 1 illustrates the voltage decay process of the battery voltage values with respect to data communication.

Equation 3 illustrates the voltage decay curve exhibited by the battery.

$$F(V) = a_1 \sin(b_1x + c_1) + a_2 \sin(b_2x + c_2) \tag{3}$$

V is the battery voltage; a_1, b_1, a_2 and b_2 are curve constants. The V_0 specification in the algorithm is chosen based on Table 1, after 3.3 V the decay becomes fast and reaches 0 rapidly. Figure 2 illustrates the EABM routing protocol.

The role of node is classified into CM, CH, effective CH, prominent CH. Effective CH handles nearby cluster data alone and prominent CH handles all network data. The role of CH is to receive data from its own cluster, aggregate and communicate to the nearby cluster. However, the effective CH also handles nearby CH with one hop distance. The prominent CH handles n hop data from all clusters inside the network. Figure 3 elucidates the sensor node role as CM and CH.

Table 1 Voltage characteristics of the battery

S. no	Voltage (V)	Number of packets sent with 5 m distance
1.	5	500
2.	5	1000
3.	5	1500
4.	4.9	2000
5.	4.9	2500
6.	4.8	3000
7.	4.8	3500
8.	4.7	4000
9.	4.7	4500
10.	4.6	5000
11.	4.6	5500
12.	4.4	6000
13.	4.3	6500
14.	4.2	7000
15.	4.0	7500
16.	4.0	8000
17.	3.8	8500
18.	3.7	9000
19.	3.55	9500
20.	3.43	10,000
21.	3.3	10,500
22.	2.8	11,000
23.	2.7	11,500

The readings are taken from (GE1653450-IS2P)—5 V, Li ion, 2300 mAh battery (WASPMOTE)
The bold indicates the threshold voltage achievement

2.3 Math model

The estimated traffic load with respect to sink distance is given in Eq. (4).

$$n = \frac{\pi R^2}{\sqrt{\Delta r}} \quad (4)$$

n = is the traffic load with respect to sink, R = total distance coverage area, r = particular distance $r \rightarrow (0, R)$.

The traffic intensity at a mean hop length h is given in Eq. (5).

$$T(r) = \frac{R^2 - r^2}{2rh} \times o \quad (5)$$

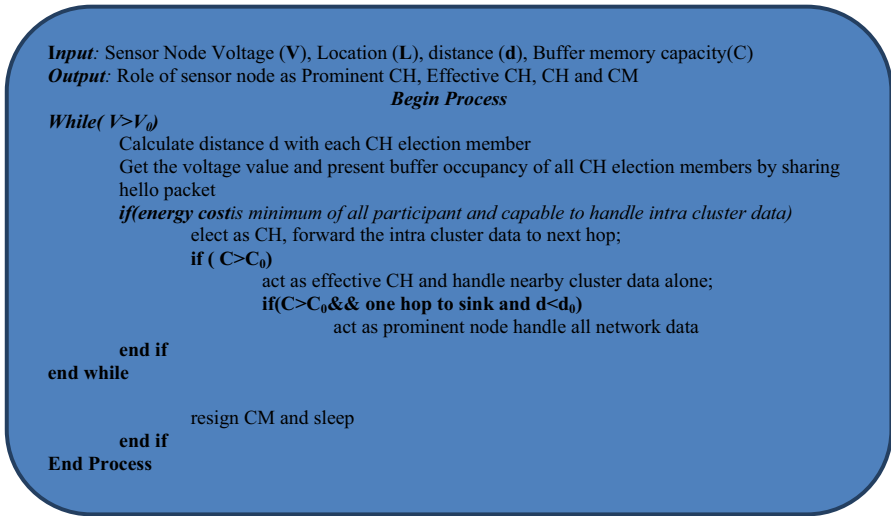


Fig. 2 EABM algorithm

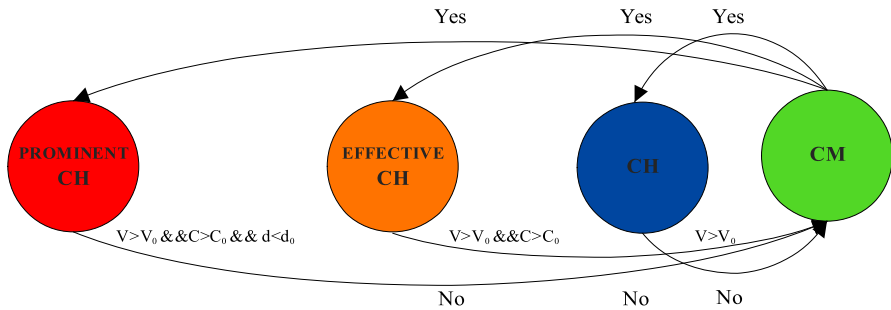


Fig. 3 Finite state machine model for CH role selection

T is the traffic of the network at r th distance, and o is the traffic rate. From Eq. (5), the traffic intensity of the network with respect to node intensity is given in Eq. (6).

$$T(r)_{total} = \int \int T(r) \rho d\theta \tag{6}$$

Figure 4 illustrates the data arrival rate with respect to the sink distance.

2.4 Hidden Markov model (HMM)

The proposed FSM has specific roles as CH and CM based on the input variable. The input variables are random in nature exhibiting memoryless property. The state transition from one state to another state is memoryless in nature. The role of node is considered to be each state with N states consisting of $S = \{PCH, ECH, CH, CM\}$ and $Q_t = \{q_1, q_2, q_3 \dots q_t\}$ as sequence at time t . The specification of HMM is given with triplet $\lambda = (A, B, \pi)$ in which A is the state transition probability matrix, B is the

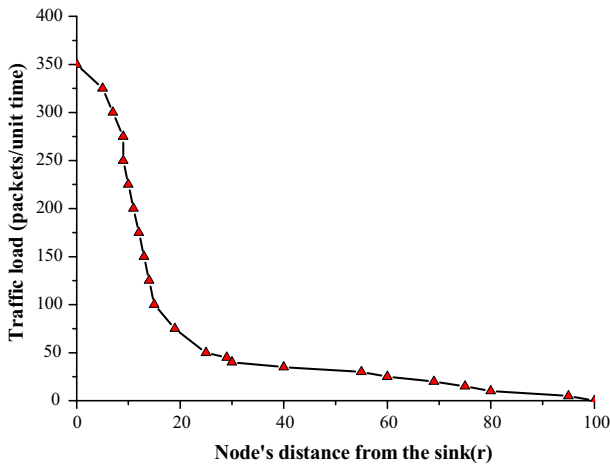


Fig. 4 Traffic load with respect to sink location

observation probability distribution and π is the initial state distribution. Equation (7) provides the probability of node to be in a particular state in the FSM.

$$A = [a_{ij}] = P(q_{t+1} = j | q_t = i) \tag{7}$$

Here, for the proposed FSM model, the state transition matrix is given in Eq. 8.

$$A = \begin{pmatrix} a_{11} & a_{12} & a_{13} & a_{14} \\ a_{21} & a_{22} & a_{23} & a_{24} \\ a_{31} & a_{32} & a_{33} & a_{34} \\ a_{41} & a_{42} & a_{43} & a_{44} \end{pmatrix} \tag{8}$$

The observability of the node in the particular state is given in Eq. (9). Equal probabilities were given to all nodes at initial stage. However, the probabilities are revised based on their battery voltage level and distance between sender and receiver.

$$B = [b_j(k)] = P(o_t = k | q_t = j) \quad 1 \leq k \leq M \tag{9}$$

3 Results and discussion

The proposed model is simulated in MATLAB with 100 nodes in 500×500 m simulation area. The following assumptions are made for simulating the proposed algorithm.

- All nodes are inside the region of interest (RoI)
- All nodes are static in nature

All nodes are homogenous with same battery capacity and the sink is powered with permanent power source. Table 2 illustrates the simulation prelims. The sink is located outside the region of interest to demonstrate the network clustering strategy.

Table 2 Simulation preliminaries

Parameters	Value
Network size	500 × 500 m ²
Number of nodes	100
Base station location	(250, 750)
E_{elec}	50 nJ/bit
E_{fs}	10 pJ/bit-m ²
Initial energy	1 J
Probability of becoming a cluster head	0.1
Data message size	2000 bytes
Header bytes	300 bytes
Buffer capacity	2 Mb

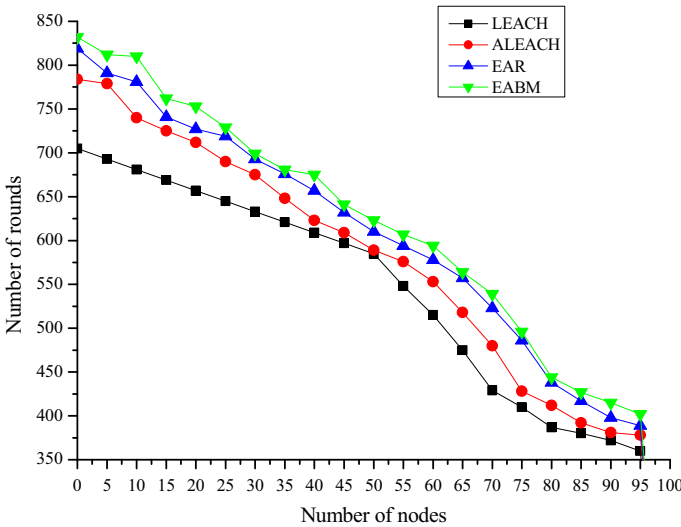


Fig. 5 Network lifetime

Figure 5 illustrates the node lifetime with respect to number of rounds. The proposed algorithm outperforms the LEACH and LEACH-C algorithms by 1.24 times and 1.14 times. The first dead node in the proposed is observed after 145 rounds, whereas in the case of LEACH and LEACH-C it is observed earlier in 124 and 138 rounds.

Figure 6 illustrates the throughput and drop packet of the proposed, LEACH and LEACH-C algorithms. The proposed algorithm outperforms the other algorithms in case of throughput and drop packet. The energy consumed due to retransmission of the same packet is also reduced in case of the proposed EABM routing protocol.

Figure 7 illustrates the memory and energy consumption of the nodes and it is observed that the memory consumption is equal and the data load is equally distributed across the network.

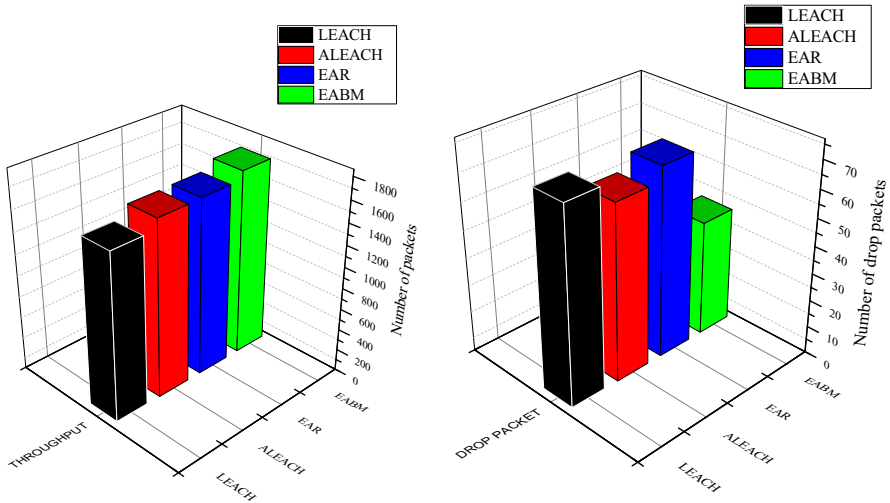


Fig. 6 Throughput and drop packet scenario

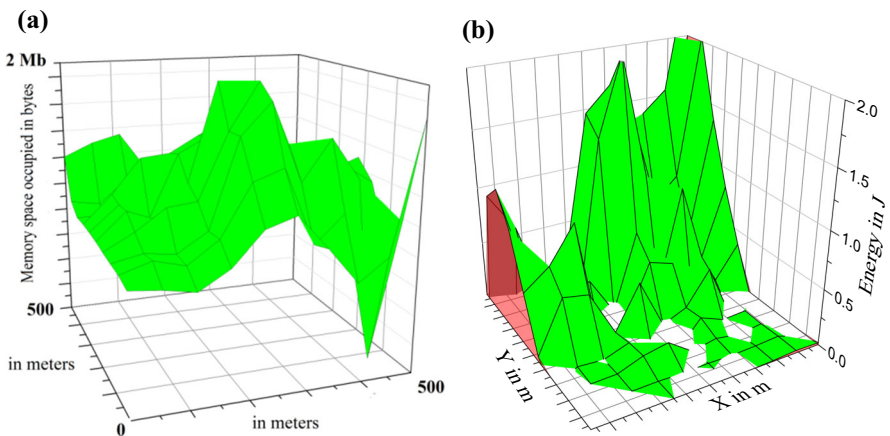


Fig. 7 Memory and energy consumption of the network during HNA. **a** Memory consumption, **b** energy level

Figure 8 illustrates the residual energy of the network after every 500 rounds. The proposed algorithm also promotes better load sharing and avoids HOTSPOT and energy hole problem in the network.

4 Conclusion

The proposed EABM algorithm serves to be a better solution for the lifetime problem in the network. The algorithm also avoids drop packet inside the network and avoids unnecessary energy consumption caused by retransmission of the same packet. The

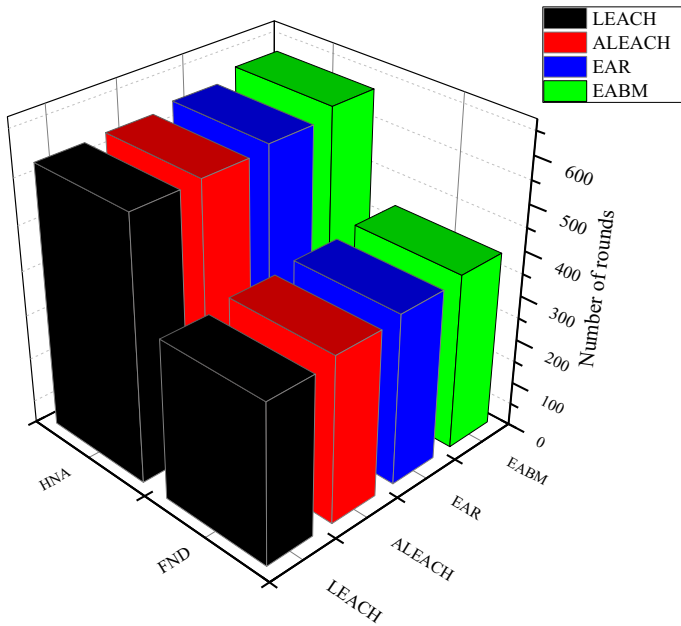


Fig. 8 Half node alive and first dead node scenario in network

load is equally shared among the network making it a solution for energy hole and HOTSPOT problem. The future work of the article will be EABM for mobile sink and multiple sink-based wireless sensor network.

References

1. Akyildiz IF, Vuran MC (2010) Wireless sensor networks, vol 4. Wiley, London
2. Rahman A, Anwar S, Pramanik I, Rahman F (2013) A survey on energy efficient routing techniques in wireless sensor networks. In: ICACT, pp 200–205
3. Chakrabarty K, Iyengar SS, Qi H, Cho E (2002) Grid coverage for surveillance and target location in distributed sensor networks. *IEEE Trans Comput* 51(12):1448–1453
4. Du X, Guizani M, Xiao Y, Chen H-H (2007) Two tier secure routing protocol for heterogeneous sensor networks. *IEEE Trans Wirel Commun* 6(9):3395–3401
5. Jin S, Li K (2009) LBSC: a load balanced clustering scheme in wireless sensor networks. In: Third International Conference on Multimedia and Ubiquitous Engineering, 2009. MUE'09, pp 221–225
6. Maheswar, R, "Performance analysis of an energy optimization scheme for cluster based heterogeneous sensor networks", Anna University Thesis, 2012
7. Maheswar R, Jayaparvathy R (2010) Performance analysis using contention based queueing model for wireless sensor networks. In: The International Congress for global Science and Technology, pp 59–59
8. Maheswar R, Jayaparvathy R (2011) Performance analysis of cluster based sensor networks using N-policy M/G/1 queueing model. *Eur J Sci Res* 58:177–188
9. Maheswar R, Jayaparvathy R (2012) Performance analysis of fault tolerant node in wireless sensor network. In: Advances in Communication, Network, and Computing: Third International Conference, CNC 2012, Chennai, India, 24–25 Feb, vol 108, pp 121–121

10. Ghaffari A (2014) An energy efficient routing protocol for wireless sensor networks using a-star algorithm. *J Appl Res Technol* 12(4):815–822
11. Mostafaai H, Obaidat MS (2018) Learning automaton-based self-protection algorithm for wireless sensor networks. *IET Networks* 7(5):353–361
12. Salehian S, Shamshiri R (2015) A survey on mobility management protocols in wireless sensor network-internet protocol. *Indian J Sci Technol* 8(11):1
13. Sasikumar P, Khara S (2012) K-means clustering in wireless sensor networks. In: 2012 Fourth International Conference on Computational Intelligence and Communication Networks (CICN), pp 140–144
14. Soua R, Minet P (2011) A survey on energy efficient techniques in wireless sensor networks. In: Wireless and Mobile Networking Conference (WMNC), 2011 4th Joint IFIP, pp 1–9
15. Tandon R, Dey B, Nandi S (2013) Weight based clustering in wireless sensor networks. In: 2013 National Conference on Communications (NCC), pp 1–5
16. Zhu C, Zheng C, Shu L, Han G (2012) A survey on coverage and connectivity issues in wireless sensor networks. *J Netw Comput Appl* 35(2):619–632
17. Yu Y, Estrin D, Govindan R (2001) Geographical and energy-aware routing: a recursive data dissemination protocol for wireless sensor networks. UCLA Computer Science Department Technical Report, UCLA-CSD TR-01-0023, May, 2001
18. Rodoplu V, Meng TH (1999) Minimum energy mobile wireless networks. *IEEE J Sel Areas Commun* 17(8):1333–1344
19. Li L, Halpern JY (2001) Minimum-energy mobile wireless networks revisited. In: Proceedings IEEE ICC'01, Helsinki, Finland, pp 278–283
20. Kanagachidambaresan GR, Chitra A (2016) TA-FSFT thermal aware fail safe fault tolerant algorithm for wireless body sensor network. *Wirel Pers Commun* 90(4):1935–1950
21. Akyildiz IF, Su W, Sankarasubramaniam Y, Cayirci E (2002) Wireless sensor networks: a survey. *Comput Netw* 38(4):393–422
22. Kanagachidambaresan GR, SarmaDhulipala VR (2014) Cardiac care assistance using self configured sensor network—a remote patient monitoring system. *J Inst Eng India Ser B* 95(2):101–106
23. Kanagachidambaresan GR, SarmaDhulipala VR, Vanusha D, Udhaya MS (2011) Matlab based modeling of body sensor network using ZigBee protocol. *CIIT* 773–776:2011
24. Nayak P, Anurag D (2016) A fuzzy logic based clustering algorithm for WSN to extend the network lifetime. *IEEE Sens J* 16(1):137–144
25. HodaTaheri et al (2012) An energy-aware distributed clustering protocol in wireless sensor networks using fuzzy logic. *Ad Hoc Netw* 10:1469–1481
26. Zhang De-gan, Liu Si, Zhang Ting, Liang Zhao (2017) Novel unequal clustering routing protocol considering energy balancing based on network partition & distance for mobile education. *J Netw Comput Appl* 88:1–9
27. Han G, Zhang C, Jiang J, Yang X, Guizani M (2017) Mobile anchor nodes path planning algorithms using network-density-based clustering in wireless sensor networks. *J Netw Comput Appl* 85:64–75
28. Muhammed T, Shaikh RA (2017) An analysis of fault detection strategies in wireless sensor networks. *J Netw Comput Appl* 78:267–287
29. Yigit M, Cagri Gungor V, Fadel E, Nassef L, Akkari N, Akyildiz IF (2016) Channel-aware routing and priority-aware multi-channel scheduling for WSN-based smart grid applications. *J Netw Comput Appl* 71:50–58
30. Ari AAA, Yenke BO, Labraoui N, Damakoa I, Gueroui A (2016) A power efficient cluster-based routing algorithm for wireless sensor networks: Honeybees swarm intelligence based approach. *J Netw Comput Appl* 69:77–97
31. Moussaoui O, Ksentini A, Naimi M, Gueroui M (2006) A novel clustering algorithm for efficient energy saving in wireless sensor networks. In: 2006 International Symposium on Computer Networks. IEEE, pp 66–72
32. Titouna C, Aliouat M, Gueroui M (2016) FDS: fault detection scheme for wireless sensor networks. *Wirel Pers Commun* 86(2):549–562
33. Srinivasan K, Dutta P, Tavakoli A, Levis P (2010) An empirical study of low power wireless. *ACM Trans Sens Netw (TOSN)* 6(2):16
34. Heidarian F, Schmaltz J, Vaandrager F (2012) Analysis of a clock synchronization protocol for wireless sensor networks. *Theor Comput Sci* 413(1):87–105

35. Yao Y, Cao Q, Vasilakos AV (2015) EDAL: an energy-efficient, delay-aware, and lifetime-balancing data collection protocol for heterogeneous wireless sensor networks. *IEEE/ACM Trans Netw (TON)* 23(3):810–823
36. Ahmed R, El-Rabaie ESM, Abd-Elnaby M, FathiAbd ES (2013) Efficient routing with compressive sensing for wireless sensor network. *INFOCOMP* 12(1):1–9
37. Shekaramiz M et al (2017) Sparse Bayesian learning using variational Bayes inference based on a greedy criterion. In: 51st IEEE Signals, Systems, and Computers (Asilomar) Conference, pp 858–862
38. Shekaramiz M, Moon TK, Gunther JH (2016) Sparse Bayesian learning boosted by partial erroneous support knowledge. In: 50th IEEE Signals, Systems and Computers, Conference, pp 389–393

Affiliations

P. Jayarajan¹ · G. R. Kanagachidambaresan² · T. V. P. Sundararajan³ · K. Sakthipandi⁴ · R. Maheswar¹ · A. Karthikeyan⁵

G. R. Kanagachidambaresan
kanagachidambaresan@gmail.com

T. V. P. Sundararajan
sundararajantvp@siet.ac.in

K. Sakthipandi
sakthipandi@gmail.com

R. Maheswar
maheshh3@rediffmail.com

A. Karthikeyan
a.karthik1982@gmail.com

- ¹ Department of ECE, Sri Krishna College of Technology, Coimbatore, India
- ² Department of CSE, Veltech Rangarajan Dr. Sagunthala R&D Institute of Science and Technology, Chennai, India
- ³ Department of ECE, Sri Shakthi Institute of Engineering and Technology, Coimbatore, India
- ⁴ Department of Physics, Sethu Institute of Technology, Virudhunagar, India
- ⁵ Department of ECE, Vel Tech Multi Tech Dr. Rangarajan Dr. Sakunthala Engineering College, Chennai, India

Accepted Manuscript

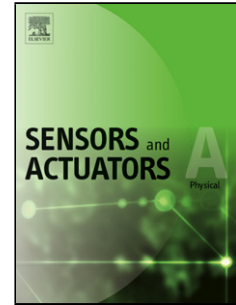
Title: Salinity Sensor Using Photonic Crystal Fiber

Authors: D. Vigneswaran, N. Ayyanar, Mohit Sharma, M. Sumathi, M.S. Mani Ranjan, K. Porsezian

PII: S0924-4247(17)31474-7
DOI: <https://doi.org/10.1016/j.sna.2017.10.052>
Reference: SNA 10418

To appear in: *Sensors and Actuators A*

Received date: 14-8-2017
Revised date: 8-10-2017
Accepted date: 20-10-2017



Please cite this article as: D.Vigneswaran, N.Ayyanar, Mohit Sharma, M.Sumathi, Mani Ranjan M.S., K.Porsezian, Salinity Sensor Using Photonic Crystal Fiber, Sensors and Actuators: A Physical <https://doi.org/10.1016/j.sna.2017.10.052>

This is a PDF file of an unedited manuscript that has been accepted for publication. As a service to our customers we are providing this early version of the manuscript. The manuscript will undergo copyediting, typesetting, and review of the resulting proof before it is published in its final form. Please note that during the production process errors may be discovered which could affect the content, and all legal disclaimers that apply to the journal pertain.

Salinity Sensor Using Photonic Crystal Fiber

D. Vigneswaran¹, N. Ayyanar², Mohit Sharma^{*,3}, M. Sumathi⁴, M.S. Mani Rajan⁵ and K. Porsezian⁶

¹ Department of Electronics and Communication Engineering, Sri Krishna College of Technology, Coimbatore, Tamilnadu India. (Email: dhasa.viki@gmail.com).

^{2,4} Department of Electronics and Communication Engineering, Dhirajlal Gandhi College of Technology, Salem, India. (Email: inrsri@gmail.com and nnsuna@yahoo.in).

³ Department of Physics, Birla Institute of Technology, Mesra, Ranchi, Jharkhand-835215, India. (Email: mohitsharmac@gmail.com and mohit@bitmesra.ac.in).

⁵ Department of Physics, University College of Engineering, Anna University, Ramanathapuram, India. (Email: senthilmanirajanofc@gmail.com).

⁶ Department of Physics, Pondicherry University, Puducherry-605 014, India. (ponzol@gmail.com).

1

Highlights

- • Unique salinity sensor employing photonic crystal fiber is designed for the first time
- • Infiltration of sea water in air holes offers high confinement loss and act as analyte core mode
- • The designed sensor exhibit high sensitivity for the determination of salinity in seawater
- • The high sensitivity for x and y-polarization is reported as 5405 and 5675 nm/RIU, respectively
- • Proposed PCF promises the large birefringence of the magnitude of 10^{-3}

Abstract — A salinity sensor employing photonic crystal fiber is designed for measuring the concentration of salt in sea water. The sea water sample is infiltrated into one of the air holes in cladding, which offers high confinement loss and act as an analyte core mode and background acts as silica mode. In order to satisfy the phase matching condition, the power transferred from silica core to the liquid filled analyte core, which is investigated using finite element method. An enhanced sensitivity of salinity in sea water reports as 5405 nm/RIU for x-polarization and 5675 nm/RIU for y-polarization with a detection limit of 0.0037 RIU has been reported. The proposed PCF also promises to yield the large birefringence of order 10^{-3} along with the enhanced sensitivity.

Keywords—Photonic crystal fiber, Salinity sensor, Coupled-mode theory, Polarization and Sensitivity.

Introduction

The photonic crystal fiber (PCF) is a leading technology in photonics departments, as it can be constructed in 1-D, 2-D and 3-D crystals and arranged with a periodic array of air holes for particular fiber length. It shows tremendous advantages over a conventional fiber, such as, a high confinement field, tunable birefringence [1], tunable dispersion, compact sensing and single mode generation for the propagation [1-10]. Additionally, the presence of air holes supports providing a modulated response in its transmission spectra within the introduction of different kind of materials such as temperature dependent liquids, wavelength dependent metallic layers [2] and so on. Recently, it has been widely used in sensing applications as the PCFs can provide appreciable levels of sensitivity to changes in refractive index. It has been reported to be used for measuring temperature [2], hydrostatic pressure [3], strain [4], vibration [5], twist [6], refractive index [7], SPR sensor [8] and magnetic field [9]. The corresponding sensor is then utilized for physical, chemical, bio-sensor applications respectively. The sensing mechanism may also be considered as an ideal application in the area of industrial process control, biochemical, and salinity detection [10-16].

Normally, the quality of pure water plays a vital role in determining the health of humans and other living organisms and it is monitored by agriculture and other industrial applications. One quality of water is the presence of salinity. Salinity is the indication of dissolved salts in seawater, usually expressed in grams per kilogram or parts per thousand by weight. The absolute salinity is defined as the ratio of mass of dissolved material in a sample of seawater. If the standard seawater has a salinity level of 35‰ at 0°C, then it is said to have average salinity. In order to quantify the concentration of salts, it is necessary to record the environmental conditions and to measure those parameters in the chemistry of the oceans [13]. During the preceding decade, optical fiber has been used for the determining the salinity level in salt solutions. Recently a PCF-based sensor has been reported to have been used for sensing solutions and providing the better detection of the given different analyte components. With the help of this capability, high index PCF has been used for many sensing applications. Using this technique, the quality of sea water has been measured [14] by Attivissimo *et al.*, later it has

been utilized for the assessment of salinity with Polyimide coated PCF [15] showing a sensitivity of 0.742 nm/mol/l and more recently, a directional coupler-based salinity sensor was reported using polyimide coated micro fibers [16].

In this study, a novel sensor based PCF's is proposed to quantify salinity where the samples for analysis will be injected, in various concentrations, into the respective cavities of the PCF where it acts as a liquid core. At the same time, the defect mode in the silica based substrate is characterized using FEM. On the formation of silica core, the diameter of left and right circle size is increased in order to induce the polarization of the propagating radiation. Because, the fiber structure is made by taking into account of multitudinous purposes, such as beam splitters, high birefringence, high sensitivity, etc. The bigger air holes on both the sides near to the centre region of PCF causes to transfer the mode field into sea water infiltrated core, which helps to satisfy the condition of resonance coupling between silica and infiltrated analyte modes. On the other hand, these two big air holes also offer high birefringence of the order of 10^{-3} over a wide range of operating wavelengths. These proposed structure is followed some experimental realization such as the infiltration of samples into PCF's air holes has been implemented by several authors using capillary force, pressure and selective filling method for the investigation of linear and nonlinear optical pulse propagation [17-19]. Yang et al. [20] have demonstrated the infiltration of glucose samples into the air holes surrounded by 60 nm of silver nanowires using LMA-PCF. Kieu et al. [21] infiltrated the mixture of CS₂ and CCl₄ using the capillary action. Recently, Wang et al. [22] discussed the different technique for the infiltration of samples by using focused ion beam milled micro-channels method. Hence, the sea water can be filled in proposed PCF based on the aforementioned experimental techniques to investigate the salinity sensor. The process for sensing is based on the shift of the wavelength of the peak of the absorption loss, which occurs due to changes in refractive index of the sensor. The refractive index change occurs when the silica core mode is coupled to the analyte mode or to the defect mode to satisfy the phase matching condition.

The refractive index of the sea water varies from 1.3326 to 1.3505 as a function of the change in salinity level from 0 to 100% at room temperature, according to Equation-2 below. We have achieved a sensitivity for the determination of salinity in seawater as 5405 nm/RIU for *x*-polarization and 5675 nm/RIU for *y*-polarization with a detection uncertainty of 0.0037 RIU.

Structure Design

The cross-sectional view of designing PCF sensor shows a silica filled the background with a uniform spacing of air holes at pitch constant $\Lambda = 2 \mu\text{m}$. For a dual-core fiber, the central hole is removed and it acts as a silica core, whereas another core is formed by injecting the sample to be analyzed into the middle cavity hole, which is located vertically in the center above the second horizontal row. The diameter of the injection hole is chosen to be $d_2 = 0.6 \mu\text{m}$. Furthermore, two air holes in horizontal direction near the center core are increased. This modification leads to the large polarization effect. Initially, the bigger air holes diameter d_1 is fixed to $2.2 \mu\text{m}$ which holds the constricted mode field confinement. For $d_1 > 2.2 \mu\text{m}$ leads to the collapse of air holes, as a result, the core of the fiber is unable to hold the mode field. Increasing the value after $2.2 \mu\text{m}$ also leads to the saturation in sensitivity as well as the wavelength shift. For $d_1 \leq 2.2 \mu\text{m}$, leads to the enhanced sensitivity with efficient mode coupling. The remaining air holes have fixed diameters, $d = 1.4 \mu\text{m}$, and provide the support for the light confinement as illustrated in the Fig.1.

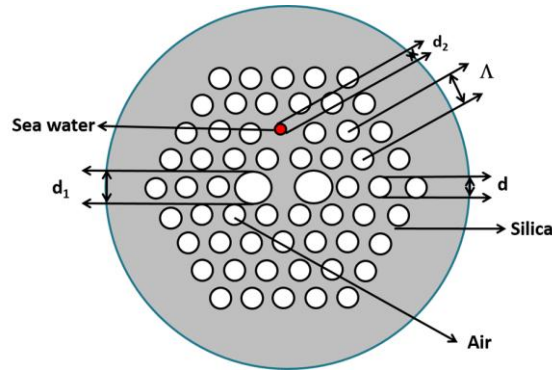


Fig.1. Cross-sectional view of the Proposed PCF sensor

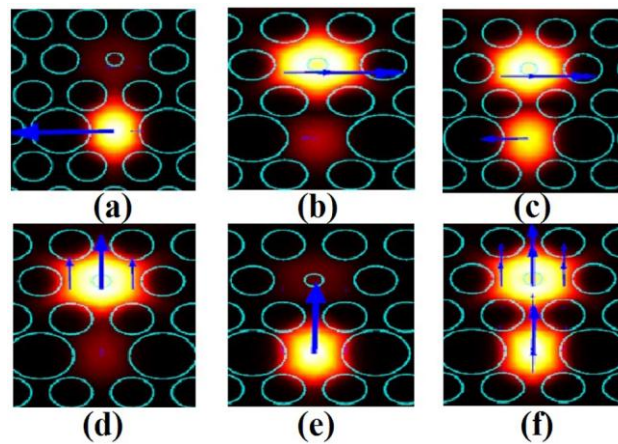


Fig.2. Electric field distributions of (a) silica core mode for x polarization, (b) defect core mode for x-polarization, (c) coupling between silica and defect core for x-polarization, (d) defect core mode for y polarization, (e) silica core mode for y-polarization, (c) coupling between silica and defect core for y-polarization. The arrow represents the direction of electric field.

The background material of the fiber is fused silica, whose refractive index at any wavelength and temperature may be calculated, using the Sellmier's equation [23], as

$$n^2(\lambda, T) = (1.31552 + 6.90754 \times 10^{-6}T) + \frac{(0.788404 + 23.5835 \times 10^{-6}T)\lambda^2}{\lambda^2 - (0.01110199 + 0.584758 \times 10^{-6}T)} + \frac{(0.91316 + 0.548368 \times 10^{-6}T)\lambda^2}{\lambda^2 - 100} \quad (1)$$

where, λ is the free space wavelength, in microns, and T is temperature, in Celsius. The refractive index of sea water as a function of the salinity obeys the following formula [24] as,

$$n(S, T, \lambda_p) = 1.3140 + (1.779 \times 10^{-4} - 1.05 \times 10^{-6} T + 1.6 \times 10^{-8} T^2)S - 2.02 \times 10^{-6} T^2 + \frac{15.868 + 0.01155S - 0.00423 T}{\lambda} - \frac{4382}{\lambda^2} + \frac{1.1455 \times 10^{-6}}{\lambda^3} \quad (2)$$

where, S is the salinity (%), and T is the temperature ($^{\circ}$ C) of the seawater, λ is the probing wavelength in nm, and n is the refractive index of the seawater represented in refractive index units (RIU).

Results and Analysis

The working principle of the salinity sensor is based on the interaction of liquid filled core with the silica based core. Light propagating in the silica core produces an evanescent field that penetrates through the cladding region to the defect core. The variation of the real and imaginary parts of the effective refractive index was studied at different concentrations of sea water injected into the PCF. The perfectly matched layer (PML) is applied to the outer circle of the PCF, which is used to absorb radiant energy from the fiber axis and prevents the reflection of stray energy. The scattering boundary condition is set with PML, which helps us to further

reduce the reflected energy. As the refractive index of the sea water is less than that of silica, various concentrations of sea water are filled-up in the small air hole ($d_2 = 0.6 \mu m$), which exhibits the confinement loss and works as a defect mode. The silica core modes, which can be controlled by birefringence are shown in the Fig.2 (a) and (e) for x and y polarization and the defect core modes are shown in the Fig.2 (b) and (d) for x and y polarization. These modes can be controlled by the liquid material. From the coupling mode theory [4], the coupling and phase matching property that occurs in the silica and defect cores for x and y polarization are shown in the Fig.2 (c) and (f), respectively. It is inferred from Fig.2 (c) and Fig.2 (f) that the coupling power will be more for y -polarization than for x -polarization.

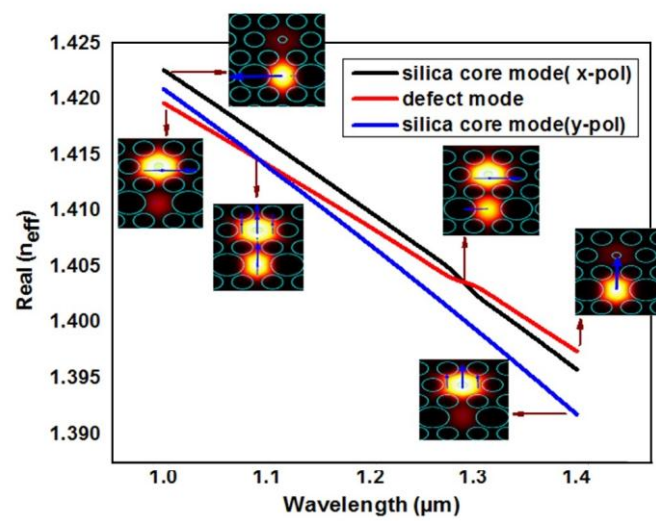


Fig.3. Effective refractive index of the silica core mode and defect mode as a function of wavelength at 40% salt level in sea water.

Fig.3 depicts the effective refractive indices of the x and y polarization of fundamental silica core mode and fundamental defect mode at salt level of concentration 40% (RI value is 1.3397) of seawater with the corresponding wavelength, λ . It is clearly shown that the refractive indices of defect mode interact with that of the silica core x and y -polarization mode at $1.32 \mu m$ and $1.1 \mu m$, respectively. For the silica core mode, maximum energy takes place in the liquid core at shorter wavelength. As wavelength increases, the field of the mode transfers from silica core to the defect core. At the crossing point, the optical power is equally distributed to both the silica and defect cores at the peak wavelength, which is then utilized in sensing applications. At the peak wavelength, the real part of the effective refractive indices of the silica core and the defect core are equal. At longer wavelengths, almost all the mode field transfers from the silica core to the defect core. For the defect mode, the region of light transition is the inverse of silica core

mode.

The imaginary part of the effective refractive index ($Img(n_{eff})$) of silica core and defect core of x and y -polarization at 40% salinity, (RI = 1.3397) is illustrated in Fig.4 as a function of wavelength. It may be observed that the intersection of the imaginary refractive index $Img(n_{eff})$ of silica and the defect core for x -polarization is occurring at a wavelength of 1.32 μm and at 1.1 μm for y -polarization. Past the intersection of these two cores, the defect cores of x and y -polarization mode gradually increase as it satisfies the phase matching condition. The increase in the concentration of salt levels in sea water leads to the increase of the refractive index. These intersection points of wavelengths can be used for achieving highly precise detection of the operating signal.

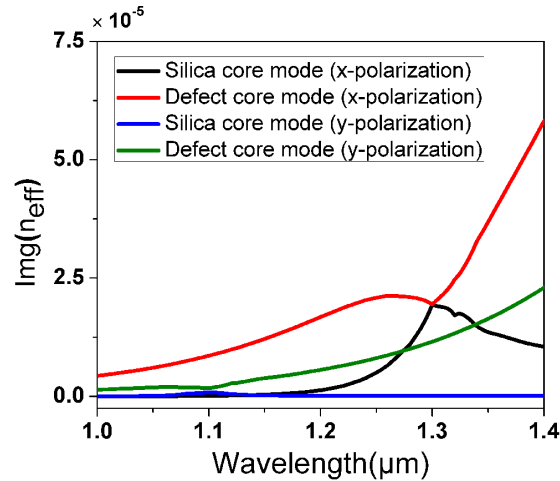


Fig.4. Imaginary part of the effective index follows the silica core and defect modes as a function of wavelength at 40% salt in the sea water.

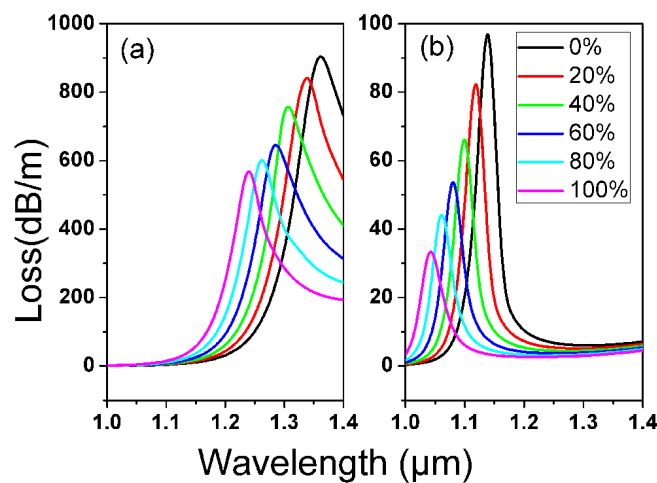


Fig.5. Confinement loss spectra of silica core mode for (a) x -polarization and (b) y -polarization under different salt level in seawater as a function of wavelength.

The confinement loss (α) plays a vital role in dual-core fibers, this can be determined by applying the following equation, $\alpha(x, y) = 8.686 \times \frac{2\pi}{\lambda} \text{Im}(n_{eff}) \times 10^6$ [4]. Fig.5 illustrates the confinement loss spectra for the silica core mode (a) x -polarization and (b) y -polarization at different concentration levels of salt in the sea water, varying from 0 to 100% as a function of wavelength (ranging from 1 μm to 1.4 μm). The resonance wavelength of confinement losses decreases as the concentration of salt levels in sea water increases, at the crossing point of the phase matching condition. It is also to be noted, that complete coupling occurs between the silica and the defect core modes as the salinity of sea water is increasing from 0 to 100%. It may also be observed that the confinement loss $\alpha(x)$ is greater than $\alpha(y)$ [18] and thus produces maximum sensing for x -polarization. The maximum is attained along the vertical direction of core mode. Such that the core mode propagation will be induced in a vertical path as it is amplified by the radius of left and right air holes. In this way, the phase matching condition for y -polarization is satisfied prior to the x -polarization. Hence, less optical power is being transferred, for x -polarization than for the y -polarization. This effect may be modified by adjusting the structural parameters of proposed sensor. Fig.5(a) depicts six peak wavelengths (λ_{peak}) at 1360, 1340, 1320, 1299, 1270 and 1240 nm for salt level of 0%, 20%, 40%, 60%, 80% and 100% in sea water for x -polarization. Thus, the λ_{peak} shifts from 1360 to 1240 nm and a maximum phase shift occurs at 120 nm for x -polarization. Similarly, one observes different maximum wavelengths of 1140, 1119, 1100, 1078, 1059 and 1039 nm for the same range of salt levels in sea water for y -polarization. The total wavelength shift is calculated as 103 nm as shown in the Fig.5 (b). The overall loss spectrum of the proposed PCF sensor also provides the conjunction of calculating the transmission spectrum, which will be found by considering the total loss of any polarization with function wavelength and also defining a specific compact of fiber length. This could be clearly express by following equations [19],

$$TR = 10 \log_{10} \left(\frac{P_o}{P_{in}} \right) \quad (2)$$

Where TR represents the optical power transmittance of PCF.

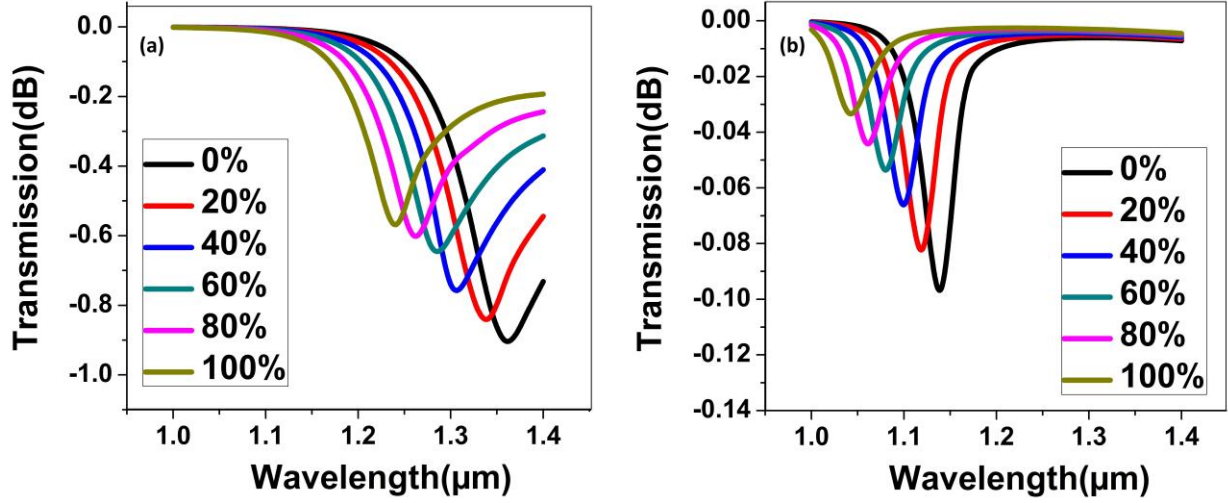


Fig.6. Optical transmittances depending on wavelength with fixed length of 1 mm salinity range from 0% - 100% (a) x-polarization. (b) y-polarization

The output power is evaluated in terms of loss is given by,

$$\frac{P_o}{P_{in}} = \exp\left(-\frac{\alpha l}{4.343}\right) \quad (3)$$

Where α represents loss spectra depending on wavelength

The corresponding length of PCF is designed as 1 mm which supports in withstand of uniform temperature, in addition, silica also provides adherent properties against any chemical substance which won't act for most acid content. The overall transmittance of proposed PCF is shown in Fig.6 for both x-polarization and y-polarization. The transmittance shows that each shift of transmission follows the inverse peak for each salinity variation. The shift variance will be the left most for the maximum salinity concentration. For example, the green curve shifts toward shorter wavelength for maximum salt (100%) concentration, whereas the black curve shifts towards longer wavelength with lower salt concentrations. Each peak of transmittance gives the minimum dip wavelength and wavelength shift between the transmission curves.

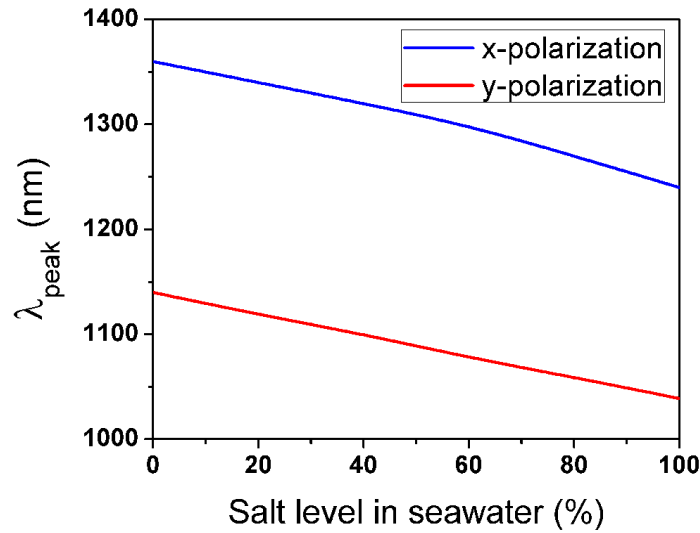


Fig.7. Peak wavelength as a function of salinity in sea water.

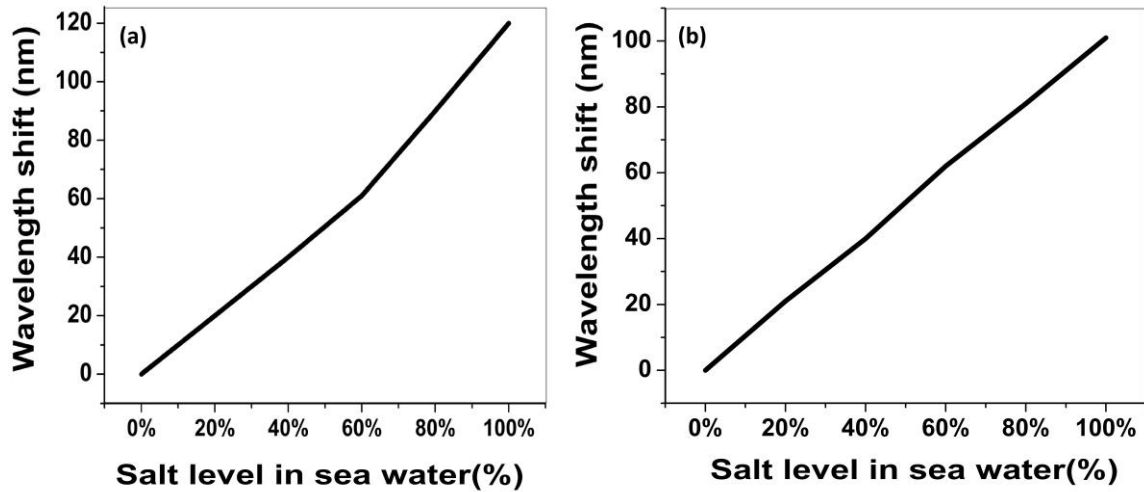


Fig.8. Wavelength of the proposed sensor with various salt levels in sea water at (a) x -polarization and (b) y -polarization.

Fig.7 depicts the λ_{peak} positions of the confinement loss spectrum of various concentration levels of salt in seawater for x and y polarization. The calculation shows that λ_{peak} changes linearly with increasing salt level in seawater from 0 to 100%, which can be used for salinity sensing applications. It can be clearly seen that the confinement loss spectrum of λ_{peak} moves towards shorter wavelengths with the increase in the concentration of salt levels in seawater and the shift is significant. In general, the sensitivity of the sensor can be measured through the shift of λ_{peak} for variation of refractive index with the salinity of seawater.

The sensitivity to the salinity of sea water can be defined as $S = \Delta\lambda_{peak}/\Delta n$, where, $\Delta\lambda_{peak}$ is the peak wavelength and Δn is the refractive index difference. In Fig.8 shows the calculated wavelength shift of the confinement loss spectrum in the fundamental silica core mode for each 20% of salt level in sea water, as the salinity increases from 0% in the proposed salinity sensor. It is calculated that the wavelength shift is 20 nm for x polarization and 21nm for y polarization at the 20% salt level in sea water. The sensitivity of the reported salinity PCF sensor is 5405 nm/RIU for x-polarization and 5675 nm/RIU for y-polarization at 20% salinity of sea water with a detection limit of 0.0037 RIU. The total phase shift is obtained from the confinement loss spectrum as 120 nm for x-polarization and 103 nm for y-polarization, as shown in Fig.7. In Table-I, the value of peak wavelengths (λ_{peak}^x and λ_{peak}^y), PCF sensitivity (S_x and S_y) for x and y-polarization, along with the refractive index difference is noted. These calculated values reveal the variation in sensitivity of x-polarization and y-polarization for different salt level concentration.

Table-1

Salt level (%)	(RIU)	λ_{peak}^x (nm)	λ_{peak}^y (nm)	S_x (nm/RIU)	S_y (nm/RIU)	Δn (RIU) $\times 10^{-2}$
0	1.3325	1360	1140	-	-	-
20	1.3362	1340	1119	5405	5675	0.37
40	1.3397	1320	1100	5509	5509	0.72
60	1.3433	1299	1078	5616	5709	1.08
80	1.3469	1270	1059	6224	5601	1.44
100	1.3505	1240	1039	6644	5592	1.80

The sensitivity has been also analyzed with respect to the variation of big air holes placed near to the centre core of the proposed PCF. The increment of d_1 increases the magnitude of birefringence upto $d_1=2.2 \mu m$. For $d_1 >2.2 \mu m$, the birefringence value start decreasing as increasing the size causes the collapse of these air holes.

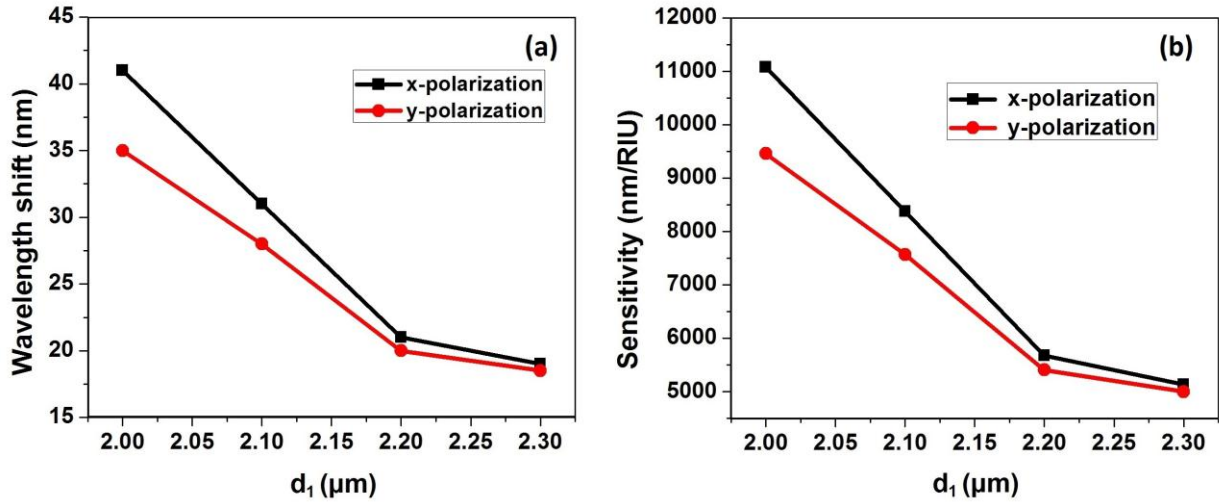


Fig.9. Variation of wavelength shift and sensitivity with varying d_1 diameters

The sensitivity and the wavelength shift are numerically analyzed with variation of d_1 and plotted in Fig.9. The wavelength shift and sensitivity is gradual decreases by increasing the values of d_1 upto $2.2 \mu m$ and starts saturating for higher values of d_1 . For example, both the wavelength shift and sensitivity is reached at its maximum level for x -polarizations as 42 nm and 11500 nm/RIU , respectively. Similarly, for y polarization it reaches at 35 nm and 9500 nm/RIU , respectively. Later, it gradually decreases with the increasing of d_1 and reaches the saturation point. It is amply clear that proposed PCF offers good sensitivity even for other values of $d_1 < 2.2 \mu m$, simultaneously decreases the magnitude of birefringence. For achieving both good sensitivity with better birefringence, it is concluded to fix the value as $d_1=2.2 \mu m$

At this point, it would be worth comparing the results with previously reported. Several authors have proposed a fiber based salinity sensor such as Possetti et al. [25], Guzman-Sepulveda et al. [26], Kamil et al. [27], and Guzman-Sepulveda et al. [28] with sensitivity of - 39 nm/RIU , 1400 nm/RIU , 2834 nm/RIU and 3485 nm/RIU , respectively. Whereas, in this work a unique type of PCF has been proposed that offer enhanced sensitivity of salinity in the seawater as 5405 nm/RIU and 5675 nm/RIU for x and y -polarization with the detection limit of 0.0037 RIU .

Conclusion

The aim of this paper was to describe a proposed salinity sensor with a very high sensitivity using a PCF and modeled by FEM. The sensing range of the proposed sensor is from 0 to 100% relative salt concentration in sea water. The sea water is injected into one of the cladding air holes in the second layer above the core which acts as a defect core mode. It was demonstrated that the optical energy is transferred from the defect core to the silica core as it satisfies the phase matching condition. This principle of detection is based on the measurement of the peak wavelength as it changes in response to the changes in the refractive index which corresponds to the changes in the salinity of seawater. The change in refractive index leads to a shift in the confinement loss spectrum and the resulting shift in the peak wavelengths. It has been shown that the design has achieved a high sensitivity for the determination of salinity in seawater. The sensitivity for x and y -polarization is reported as 5405.4 nm/RIU and 5675.67nm/RIU, respectively. The detection limit of the refractive index changes was found to be 0.0037 RIU. The proposed PCF also offers the high birefringence of the magnitude 10^{-3} along with the enhanced sensitivity.

References

- [1]. M. Sharma, N. Borogohain and S. Konar. "Index guiding photonic crystal fibers with large birefringence and walk-off." *IEEE J. Lightwave Tech.*, vol. 31, no. 21, pp. 3339-3344, 2013.
- [2]. H. L. Chen, S. G. Li, J. S. Li, Y. Han, and Y. D. Wu, "High sensitivity of temperature sensor based on ultra-compact photonics crystal fibers," *IEEE Photon. J.*, vol. 6, no. 6, 2014, 6803006.
- [3]. N. Ayyanar, D. Vigneswaran, M. Sharma, M. Sumathi, MS Mani Rajan, and S. Konar. "Hydrostatic Pressure Sensor Using High Birefringence Photonic Crystal Fibers." *IEEE Sensors J.*, vol. 17, no. 3, pp. 650-656, 2016.
- [4]. J. Villatoro, V. Finazzi, V. P. Minkovich, V. Pruneri and G. Badenes, "Temperature-insensitive photonic crystal fiber interferometer for absolute strain sensing," *Appl. Phys. Lett.*, vol. 91, no. 9, 2007, 091109.
- [5]. A. Ana M. R. Pinto and M Lopez-Amo, "Photonic Crystal Fibers for Sensing Applications," *J. Sensors*, vol. 2012, pp. 1-21, 2012.

- [6]. Z. Peng, C. C. Chan, Y. Jin, T. Gong, Y. Zhang, L. H. Chen, and X. Dong. "A temperature-insensitive twist sensor by using low-birefringence photonic-crystal-fiber-based Sagnac interferometer," *IEEE Photon. Tech. Lett.*, vol. 23, no. 13, pp. 920–922, 2011.
- [7]. Du C, Wang Q, Wang X, et al. High Sensitivity Internal Refractive Index Sensor based on a Photonic Crystal Fiber Long Period Grating. *Instrumentation Science & Technology*, 2016.
- [8]. Yang X, Lu Y, Wang M, et al. SPR Sensor Based on Exposed-Core Grapefruit Fiber with Bimetallic Structure. *IEEE Photonics Technology Letters*, 2016, 28(6):649-652.
- [9]. H. L. Chen, S. G. Li, J. S. Li, and Z. K. Fan, "Magnetic field sensor based on magnetic fluid selectively infilling photonic crystal fibers," *IEEE Photon. Tech. Lett.*, vol. 27, no. 7, pp. 717–720, 2015.
- [10]. D. Clerc, and W. Lukosz. "Integrated optical output grating coupler as biochemical sensor." *Sens. and Actu. B: Chem.*, vol. 19, no. 1-3, pp. 581-586, 1994.
- [11]. IUPAC, *Compendium of Chemical Terminology*, 2nd edn., Blackwell Scientific Publications Oxford, 1997.
- [12]. F. Adamo, F. Attivissimo and C. G. C. Carducci "A small sensor network for sea water quality monitoring" *IEEE Sensors J.*, vol. 15, no. 5, pp. 2514 – 2522, 2015
- [13]. Y. Zhao and Y. Liao. "Novel Optical Fiber Sensor for Simultaneous Undersea Temperature and Salinity Measurement" *Acta Opt. Sin.*, vol. 10, no. 17, 2002.
- [14]. F. Attivissimo, C. G. C. Carducci, A. M. L. Lanzolla, A. Massaro, and M. R. Vadrucchi, "A Portable Optical Sensor for Sea Quality Monitoring", *IEEE Sensors J.*, vol. 15, no. 1, 2015.
- [15]. C. Wu, B. Guan, C. Lu, and H. Tam, "Salinity sensor based on polyimide-coated photonic crystal fiber", *Opt. Exp.*, Vol. 19, No. 21, 2011.
- [16]. S.Wang, Y.Liao, H.Yang, X.Wang, and J.Wang, "Modeling seawater salinity and temperature sensing based on directional coupler assembled by polyimide-coated micro/nano fibers", *Appl. Opt.*, vol. 54, no. 34, 2015.
- [17]. S. Kedenburg, T. Gissibl, T. Steinle, A. Steinmann, and H. Giessen, "Towards integration of a liquid-filled fiber capillary for supercontinuum generation in the 1.2–2.4 μm range", *Opt. Exp*, vol. 23, 8281 (2015)

- [18]. K. Nielsen, D. Noordegraaf, T. Sørensen, A. Bjarklev, and T. P. Hansen, "Selective filling of photonic crystal fibres", *J. Opt. A: Pure Appl. Opt.* 7 (2005) L13–L20
- [19]. C. J. S. de Matos, C. M. B. Cordeiro, E. M. dos Santos, J. S. K. Ong, A. Bozolan, and C. H. B. Cruz, "Liquid-core, liquid-cladding photonic crystal fibers", *Opt. Exp*, 15, 11207 (2007).
- [20]. X.C. Yang, Y. Lu n, M.T. Wang, J.Q. Yao, "A photonic crystal fiber glucose sensor filled with silver nanowires", *Optics Communications* 359 (2016) 279–284..
- [21]. K. Kieu, L. Schneebeli, R. A. Norwood, and N. Peyghambarian, "Integrated liquid core optical fibers for ultra efficient nonlinear liquid photonics," *Opt. Express*, vol 20, No. 7, 8148, 2012
- [22]. F. Wang, W. Yuan, O. Hansen, and O. Bang, "Selective filling of photonic crystal fibers using focused ion beam milled microchannels," *Opt. Exp.*, vol. 19, no. 18, pp. 17585–17590, 2011
- [23]. Qiang Liu, Shuguang Li, Hailiang Chen, Jianshe Li, and Zhenkai Fan, "High-sensitivity plasmonic temperature sensor based on photonic crystal fiber coated with nanoscale gold film" , *IOP science , Applied Physics Express* 8, 046701 (2015).
- [24]. X. H. Quan, and E. S. Fry, "Empirical equation for the index of refraction of seawater," *Appl. Opt.*, vol. 34, pp. 3477–3480, 1995.
- [25]. G R C Possetti, R C Kamikawachi, C L Prevedello, M Mullerand J L Fabris, "Salinity measurement in water environment with a long period grating based interferometer," *Measurement Science and Technology*, Vol.20, PP. 1-6, 2009.
- [26]. Jose R. Guzman-Sepulveda, Jaime A. Arredondo-Lucio, Walter Marugulis, Daniel A. May- Arrioja, "Salinity sensor using a two-core optical fiber," *Frontiers in optics*, OSA, 2012.
- [27]. Y. Mustapha Kamil, M.H. Abu Bakar, A. Syahir, M.A. Mahdi, "Determining salinity using a single mode tapered optical fiber," *IEEE- International conference on photonics (ICP)*, 2014.
- [28]. J.R. Guzman-Sepulveda, R.G. Cabrera, M.T. Cisneros, J.J.S. Moundragon, D.A.M. Arrioja, "A highly sensitive fiber optic sensor based on two – core fiber for refractive index measurement," *Sensors*, Vol. 13, PP. 14200-14213, 2013.

Author's Biographies



D. Vigneswaran was born in 1989. He has completed his B.E. in Electronics and Communication in 2010 from Kamaraj College of Engineering and

Technology and Master of Engineering in Optical communication at Alagappa Chettiar College of Engg and Tech, Anna University in 2015. He has published 5 paper in refereed national/international journals and more than 15 papers in conferences. His research interest includes few mode fiber design (LP ring core fiber and OAM fiber), few mode amplifier system design and sensing using ring core fiber and PCF.



N. Ayyanar was born in 1992. He has completed his B.E. in Electronics and Communication in 2013 from Narasu's sarathy institute of technology, salem, India and Master of Engineering in Optical communication at Alagappa Chettiar College of Engg and Tech, Anna University in 2015, karaikudi, India. He currently is working in Assistant professor at Dhirajlal Gandhi College of technology, salem, India. He has published 4 paper in refereed national/international journals and more than 12 papers in conferences. His research interest includes optical fiber sensor in PCF, few mode fibers and few mode amplifier system designs.



Mohit Sharma received M.Sc (Physics) specialization in Electronics from Dr. Bhim Rao Ambedkar University, Agra and Ph.D. from Department of Physics, Birla Institute of Technology, Mesra, Ranchi. He has published several research findings in reputed international journals and in international conference proceedings. He has worked on several projects in Indian Institute of Technology, Kharagpur, where he was involved in to develop Electronic nose and vision for aroma detection and in another project, he has contributed to develop data acquisition system (DAQ) (software and hardware) for geotechnical instruments. He was awarded with several national level scholarships like Sahara India scholarship in 2003, Indian Railway academic scholarship in 2002, 2004, 2007 and 2009. He joined in several research societies like IEEE as member, OSA and SPIE as a student member. He also served as a reviewer of several reputed international journals like IEEE Journal of Quantum Electronics, IEEE Sensors Letters, IEEE Journal of Lightwave Technology, Applied Optics, Journal of Physics D: Applied Physics, Nanotechnology, Journal of Optics, Journal of Nanophotonics, Optical and Quantum Electronics, Optical Engineering, Journal of Modern Optics, etc. He earned Outstanding Reviewer Award-2016 from Journal of Optics (IOP) and appreciation from several international journals. His research interests include nonlinear optics, fiber optics, photonic crystal fiber, supercontinuum generation, soliton generation, optical communication and fiber optic sensors.



M. Sumathi received the B.E degree in Electronics and Communication Engineering from PSG College of Technology, Coimbatore, India in 1992 and the M.E degree in Optical Communication from College of Engineering, Chennai, India in 2004 and her doctoral degree in the area of optical networks from Anna University, Chennai, India in the year 2010. She was a recipient of the post graduate scholarship, sponsored by the government of India, from 2002 to 2004. She is currently the Head of the ECE department at Dhirajlal Gandhi College of Technology, Salem, India. She has a total of 21 years of experience which includes industrial experience of 5 years

and teaching experience of 16 years. She was awarded ‘Senior Woman Educator and Scholar’ by NFED (National Foundation for Entrepreneurship Development) in the year 2016. Her research interest includes WDM networks, optical communication, fiber optic sensors, computer networks and wireless communication.



M.S. Mani Rajan received his B.Sc and M.Sc degree in Physics from Madurai Kamaraj University, Madurai, Tamilnadu, India. He received M.Phil from Bharathidasan University, Tiruchirappalli, India. He received Ph.D in from Anna University, Chennai. He published over 13 papers in the field of soliton based optical fiber communication systems in highly reputed international journals and he published more than 20 papers in various international conferences. He is a Life member of Indian Physics Association (IPA), Member in Indian Laser Association (ILA) and Photonics society of India (PSI). He is currently working as Assistant Professor in the Department of Physics, Anna University, University College of Engineering Ramanathapuram, Tamilnadu, India. His area of research is soliton propagation in various nonlinear waveguides, photonic crystal fiber and erbium doped fiber. He proposed many novel methods for generation of ultrashort pulses and optical solitons for different applications.



K. Porsezian was born in Gudiyattam, India, on June 5, 1963. He received the M.S. degree from the University of Madras, Chennai, India, in 1985, and the Ph.D. degree from Bhrathidasan University, Tiruchirappalli, India, in 1991. After working as a Research Scientist with the Science and Engineering Research Council, Department of Science and Technology, Government of India Project, in 1993, he joined the Department of Physics, Anna University, Chennai, as a Lecturer. He is currently a Professor with the Department of Physics, Pondicherry University, Puducherry, India. He has published more than 120 papers and edited four books on optical solitons. His current research interests include solitons and modulational instability in nonlinear fiber optics, self-induced transparency solitons, nonlinear pulse propagation in periodic structures and photonic crystal fibers, and integrability aspects of nonlinear partial differential equations. Dr. Porsezian has been a recipient of the Indian National Science Academy Young Scientists Award of the Year 1995, the Deutscher Akademischer Austauschdienst Post-Doctoral Fellowship from 1995 to 1997, the Anil Kumar Bose Memorial Award by the Indian National Science Academy in 1998, the Sathya Murthy Memorial Award of the Year in 1998 given by the Indian Physics Association, Junior and Regular Associateship Award from 1995 to 2002, the All India Council of Technical Education Career Award for Young Teachers from 1998 to 2001, the University Grants Commission Research Award from 2004 to 2007, and Department of Science and Technology Ramanna Fellowships from 2006 to 2009. He is a Program Advisory Committee Member and Fund for Improvement of Science and Technology Infrastructure Member of the Department of Science and Technology, Government of India.



Modified energy minimization scheme using queue threshold based on priority queueing model

P. Jayarajan¹ · R. Maheswar¹ · G. R. Kanagachidambaresan²

Received: 19 September 2017 / Revised: 8 December 2017 / Accepted: 15 December 2017
© Springer Science+Business Media, LLC, part of Springer Nature 2017

Abstract

A wireless sensor network (WSN) is a group of specialized sensor nodes with a communication infrastructure intended to monitor and record conditions at diverse locations. The critical issue in WSNs is represented by the limited availability of energy within the network and hence optimizing energy consumption is very important. One important existing technique used to prolong the network lifetime of WSN is the Energy Minimization Scheme (EMS) using N-Policy Model (NPM) based on queue threshold but this technique increases mean delay. This paper proposes a Modified Energy Minimization Scheme (MEMS) which reduces the mean delay and average energy consumption of individual nodes in the cluster based heterogeneous sensor network using queue threshold based on M/D/1 Priority Queueing Model (PQM) in order to prolong the network lifetime. The expression for the optimal value of queue threshold for which the node consumes minimum energy using PQM is also derived. Results show that the mean delay is highly reduced in PQM when compared to the NPM and the trade-off exist between the average energy consumption and mean delay is explored. We perform simulations and the results obtained show that the simulation results match with the analytical results thus validating the accuracy of the approach.

Keywords Queue threshold · Energy · Mean delay · PQM · NPM

1 Introduction

Wireless Sensor networks have been visualized to have a full extent of applications in military and non-military domains [1]. Many researchers have found out several aspects of wireless sensor networks such as collaborative data gathering, MAC and routing. Energy efficiency is a vital design objective in most of the research which is related to wireless sensor networks. Clustering is one important technique by which the lifetime of the network is increased. Several authors have proposed many works related to the formation of cluster and electing the CH in a cluster. The authors in [2] have pro-

posed energy efficient routing between CHs which is also highly important to prolong the network lifetime.

Clustered Sensor networks is mainly segregated into two major types; homogeneous and Heterogeneous Sensor Networks (HSNs). In homogeneous networks all the sensor nodes are unique in terms of energy in battery and complexity in the hardware [3]. The disadvantage of using a homogeneous network and role rotation is that all the nodes should possess the required hardware capabilities and also to be capable of acting as cluster heads [4,5]. The next classification, HSNs comprises of two physiologically different types of sensor nodes and most of the research papers deliver HSNs can significantly improvise the sensor network performance in dealing with energy consumption [6].

In HSN, a little number of powerful high-end sensors (H-sensors) and a more number of low-end sensors (L-sensors) are been uniformly distributed in the field. After the deployment process, clusters are been formed and the H-sensor in each of the cluster serves as Cluster Head (CH). Figure 1 provides information regarding cluster formation in HSN. Here, the small circles denote L-sensors, and large circles denote H-sensors and the large triangle present at the top-right corner denote the Base Station (BS). Powerful H-sensors which

✉ P. Jayarajan
pjayarajan@gmail.com

R. Maheswar
maheshh3@rediffmail.com

G. R. Kanagachidambaresan
kanagachidambaresan@gmail.com

¹ Department of ECE, Sri Krishna College of Technology, Coimbatore, India

² Department of CSE, Veltech Rangarajan Dr. Sagunthala R&D Institute of Science and Technology, Chennai, India

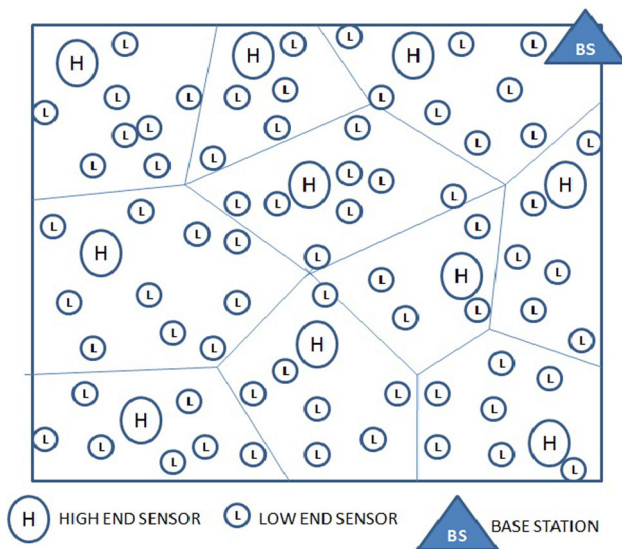


Fig. 1 Cluster formations in HSN

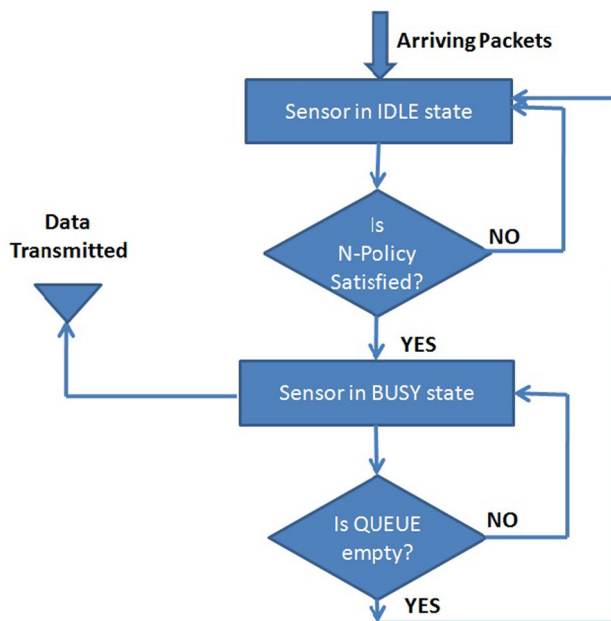


Fig. 2 Flowchart of L-sensor node's transition

serves as CH requires more supply of energy and higher transmission range than L-sensors. The more basic idea of routing in HSNs is to make each L-sensor to send its data to its CH. A CH gathers data from multiple L-sensors and delivers the data to the BS. An energy minimization technique based on queue threshold is shown in Fig. 2 which is an existing model that is widely used technique for delay insensitive WSN applications to prolong the network lifetime of HSN [7–12].

The existing EMS based on queue threshold [7–12] increases mean delay though the energy consumption is less and the network lifetime is increased. This method is suitable only for delay insensitive applications which are very few in

the current scenario of WSN applications. As most of the real time WSN applications are delay-sensitive, this method cannot be applied for delay sensitive applications since this method produces higher delay.

In this paper, a HSN is considered where clusters are formed as shown in Fig. 1. In each cluster, H-sensor act as Cluster Head (CH) and L-sensors act as Cluster Members (CM). Here, we propose a Modified Energy Minimization Scheme (MEMS) which reduces the average energy consumption of individual nodes in the cluster based HSN using queue threshold based on M/D/1 Priority Queueing Model (PQM) in order to prolong the network lifetime of the network. We develop an analytical model of a cluster based HSN using queue threshold based on M/D/1 Priority Queueing Model (PQM). The performance of the proposed model is analysed in terms of average energy consumption and mean delay. The performance analysis of the proposed MEMS is the first analytical model that specifically represents the node's behaviour in IDLE state and BUSY state during its period of active time using queue threshold based on PQM and the network performance in terms of mean delay and average energy consumption is investigated by considering prioritization of packets. We also derive the expression for the optimal value of queue threshold (N^*) for which the node consumes minimum energy.

The rest of this paper is organized as follows. In Sect. 2, we present the system model. In Sect. 3, we present the performance analysis and provide numerical solutions for determining the mean delay, average energy consumption of a sensor node in a cluster and the optimum queue threshold value (N^*) using queue threshold based on M/D/1 Priority Queueing Model (PQM). Section 4 describes the simulation model and the results and discussion are presented in Sect. 5. In Sect. 6, we provide the conclusions and future work.

2 System model

In HSN, a single cluster considered for analysis is represented in Fig. 3. In this cluster, during each node's period of active time, the L-sensors present in all clusters will be in IDLE state or BUSY state [7–12]. In this type of network, depending upon the critical information of the packet, it is classified into High Priority (HP) or Low Priority (LP) packet i.e., the packets with critical information are considered as HP packets and the packets without critical information are considered as LP packets. Since the HP packets need to be serviced immediately, it is considered under no threshold condition ($N = 1$) and the LP packets which can manage delay is considered under NPM. The sensor node will move from IDLE state to BUSY state immediately if it receives a HP packet and it will wait for threshold number of LP packets (N) to move from IDLE state to BUSY state. The node always

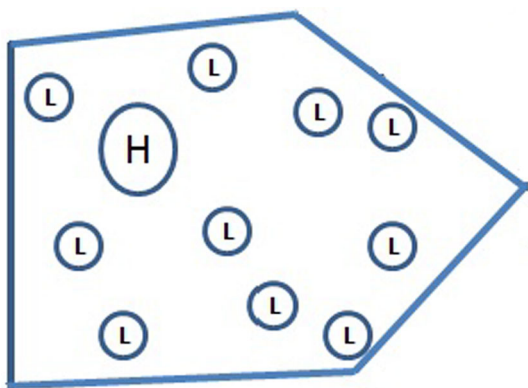


Fig. 3 A cluster in HSN

returns from BUSY state to IDLE state whenever the queue is empty. In this scenario, an assumption is been made that there is no channel contention since all the L-sensor nodes are scheduled with unique active time. The switching actions between IDLE state to BUSY state and BUSY state to IDLE state are implied to as transitions. For analysis purpose, the following assumptions are been made:

- All L-sensor nodes in a HSN are identical
- All H-sensor nodes in a HSN are identical
- The arrival of data packets to L-sensor nodes is assumed to follow a Poisson process with mean arrival rate per node (λ)
- λ_1 and λ_2 are the arrival rate of LP and HP packets where $\lambda = \lambda_1 + \lambda_2$
- Packets are delivered from L-sensor node to CH with mean service time ($1/\mu$)
- Buffer is assumed to be empty whenever the sensor node switches from sleep to active state
- There is no channel contention

3 Performance analysis

As described in Sect. 2, in this cluster, during each node’s period of active time, the L-sensors present in all clusters will be in IDLE state or BUSY state. The flow chart representing the transition status of an L-sensor node from IDLE to BUSY state and BUSY to IDLE state in MEMS is shown in the Fig. 4.

The performance of the single L-sensor node is analyzed based on M/D/1 PQM in terms of the following parameters.

3.1 Mean delay

Mean delay experienced by the packets in an L-sensor node is defined as the average waiting time of the packets in the

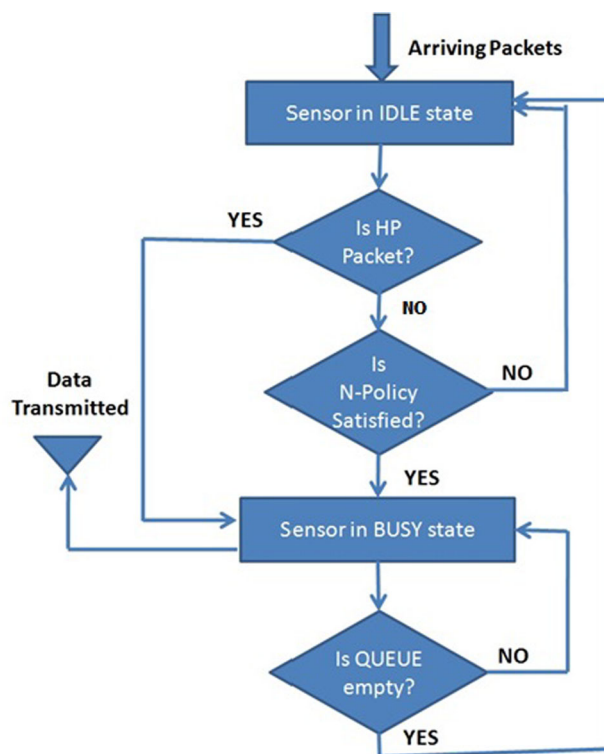


Fig. 4 Flowchart of L-sensor node’s transition based on PQM

queue. Considering an M/D/1 PQM, the mean number of LP and HP in the queue (L_1 and L_2) is given by

$$L_1 = \frac{N - 1}{2} + \frac{\rho_1 (2 - \rho_1)}{2(1 - \rho_1)} \tag{1}$$

$$L_2 = \frac{\rho_2 (2 - \rho_2)}{2(1 - \rho_2)} \tag{2}$$

where

$$\rho_1 = \frac{\lambda_1}{\mu}, \quad \rho_2 = \frac{\lambda_2}{\mu}$$

L_1 Mean number of LP packets in the L-sensor node’s buffer

L_2 Mean number of HP packets in the L-sensor node’s buffer

N Threshold number of packets

λ_1 Mean arrival rate of Low priority per node

λ_2 Mean arrival rate of High priority per node

μ Mean service rate

The mean waiting time of the LP and HP packets in the queue (W_{q1} & W_{q2}) is given by,

$$W_{q1} = \frac{N - 1}{2\lambda_1} + \frac{\rho_1}{2(\mu - \lambda_1)} \tag{3}$$

$$W_{q2} = \frac{\rho_2}{2(\mu - \lambda_2)} \tag{4}$$

3.2 Average energy consumption of an L-sensor node

The average energy consumption of LP and HP in L-sensor node $E_1(N)$ and $E_2(N)$ can be expressed as

$$E_1(N) = C_H \left(\frac{N-1}{2} + \frac{\rho_1}{1-\rho_1} \right) + C_T \left(\frac{\lambda_1(1-\rho_1)}{N} \right) \quad (5)$$

$$E_2(N) = C_H \left(\frac{\rho_2}{1-\rho_2} \right) + C_T (\lambda_2(1-\rho_2)) \quad (6)$$

where

N_{cy1} Number of cycles per unit time of LP packets

N_{cy2} Number of cycles per unit time of HP packets

and it is given by

$$N_{cy1} = \left(\frac{\lambda_1(1-\rho_1)}{N} \right) \quad (7)$$

$$N_{cy2} = \lambda_2(1-\rho_2) \quad (8)$$

C_H Energy consumption due to transmission of a packet from an L-sensor node to CH in joules

C_T Energy consumption due to transitions and synchronization in joules

The average energy consumption is given by $E(N) = E_1(N) + E_2(N)$

3.3 Optimal threshold value (N^*) of N

The optimal threshold value (N^*) is the value of N for which the sensor node consumes a minimal amount of energy and it is given by

$$N^* = 0.5 \left[\sqrt{\frac{8C_T\lambda_1(1-\rho_1)}{C_H} + 1} - 1 \right] \quad (9)$$

4 Simulation model

In this section, the simulation model is presented. Mica2 mote specifications are considered for forming a cluster based HSN. Simulations are performed for a cluster based HSN by assuming various parameters as mentioned in Tables 1, 2 and 3 [7–13].

The values of C_T and C_H from Tables 1, 2 and 3 are determined as $C_T = 6.9$ mJ and $C_H = 0.8$ mJ [7–13]. The Results are obtained by changing the threshold number of packets and mean arrival rate per node with $p = 0.1$ and $p = 0.2$ in order

Table 1 Cluster specifications

Mean arrival rate per node (packets/s)	2–20
Probability of HP packets (p)	0.1–0.5
Mean service time per packet (msec)	15
Number of L-sensor nodes in a cluster	10
Number of H-sensor nodes in a HSN	10
Number of clusters in a HSN	10
Threshold number of packets	1–20

Table 2 Time and current specification of mica2 mote

Operation	Time (s)	I (mA)
Initialize radio	350E–6	6
Turn on radio	1.5E–3	1
Switch to Transmit mode	250E–6	15
Transmit 1 byte	416E–6	20

Table 3 Power and other specifications

Battery (V)	3
Data rate (Kbaud)	38.4
Preamble length (bytes)	271
Packet length (bytes)	36
Radio off (μ A)	20

Table 4 Arrival rate versus mean delay

Arrival rate λ	Mean delay (msec) at N^*		
	PQM (p = 0.1)	PQM (p = 0.2)	NPM
5	0.056	0.114	701
10	0.113	0.229	551

to determine the mean delay, average number of cycles per second and average energy consumption of an L-sensor node in a cluster. Simulation results show that the average number of cycles per second and the average energy consumption is more in PQM when compared to NPM but the mean delay is less in PQM when compared to NPM. Meanwhile, minimal amount of energy is consumed for optimal threshold value N^* . It is observed that the (%) saving in energy consumption is maximum for the optimal threshold value. The trade-off that exists between the mean delay and the average energy consumption per node with respect to the value of N is also explored for MEMS.

5 Results and discussion

In this section, the simulation and analytical results are shown. The simulation and analytical results are obtained by

Fig. 5 Queue threshold (N) versus average number of cycles/sec

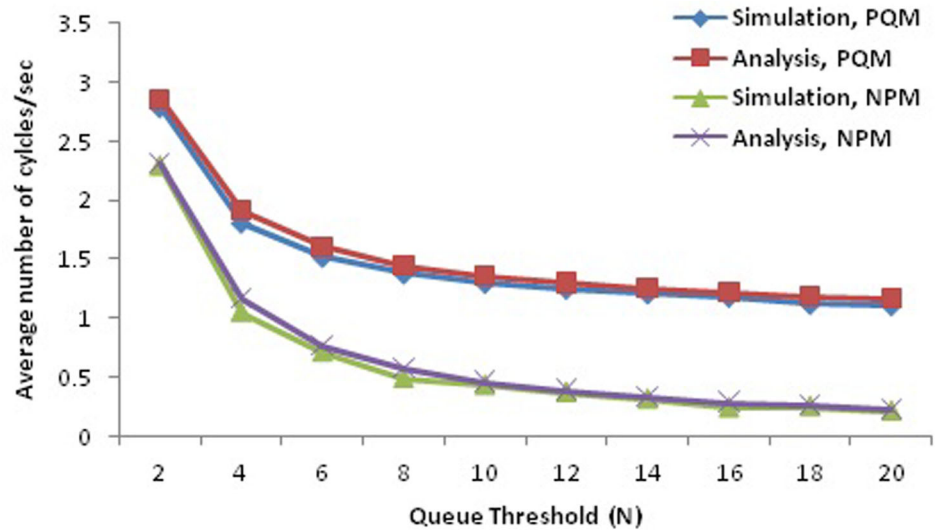
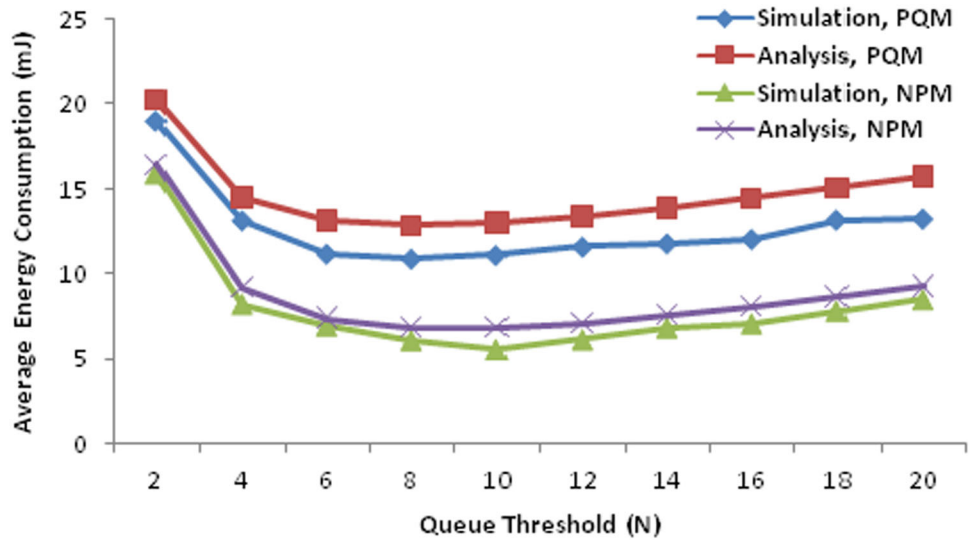


Fig. 6 Queue threshold (N) versus Average energy consumption (mJ) showing minimum energy consumption at optimal threshold



changing the threshold number of packets and mean arrival rate per node in order to determine the mean delay and number of cycles per second and average energy consumption of an L-sensor node in a cluster using NPM and PQM. From the Table 4, simulation results show that the mean delay is very less in PQM when compared NPM at optimal threshold value N^* for mean arrival rate per node as 5 and 10 packets/s. This is due to the reason that HP packets in PQM are not buffered and transmitted immediately whereas the packets in NPM is buffered until the queue threshold value and the packets are transmitted after the queue threshold is reached.

From the Fig. 5, it is observed that, when threshold (N) increases, the number of cycles increases in PQM when compared to NPM for mean arrival rate per node as 5 packets/s. This is because the HP packets are transmitted immediately without buffering which increases the number of transitions. Here, the average number of cycles per second reduces as

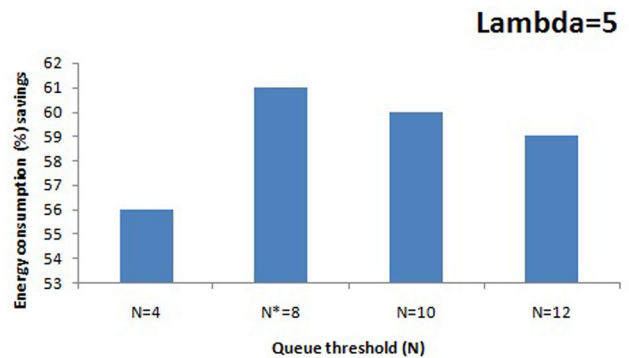


Fig. 7 Queue threshold (N) versus Energy consumption savings (%)

the value of N increases because the transitions from IDLE state to BUSY state and vice versa in an L-sensor node is less when the queue threshold is high because the time taken for the buffer to be filled with threshold number of packets for

Table 5 Arrival rate versus average energy consumption

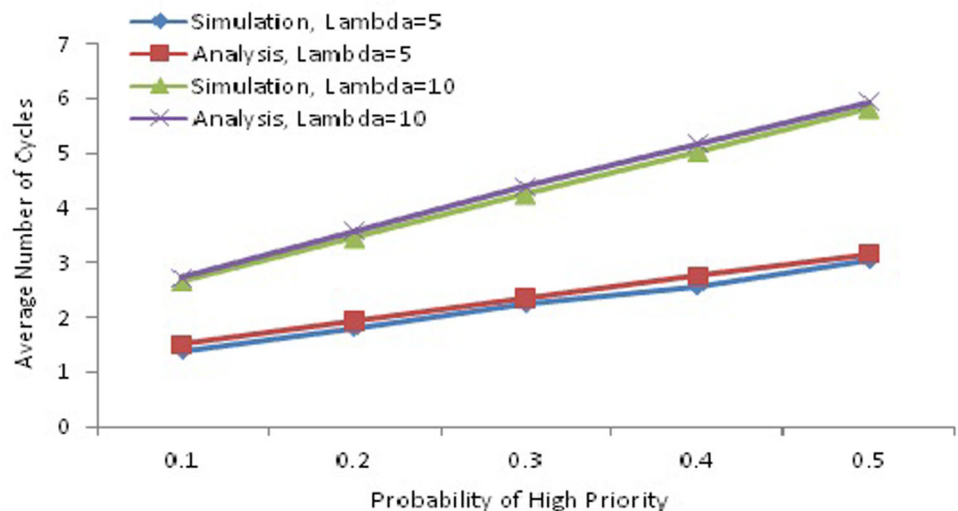
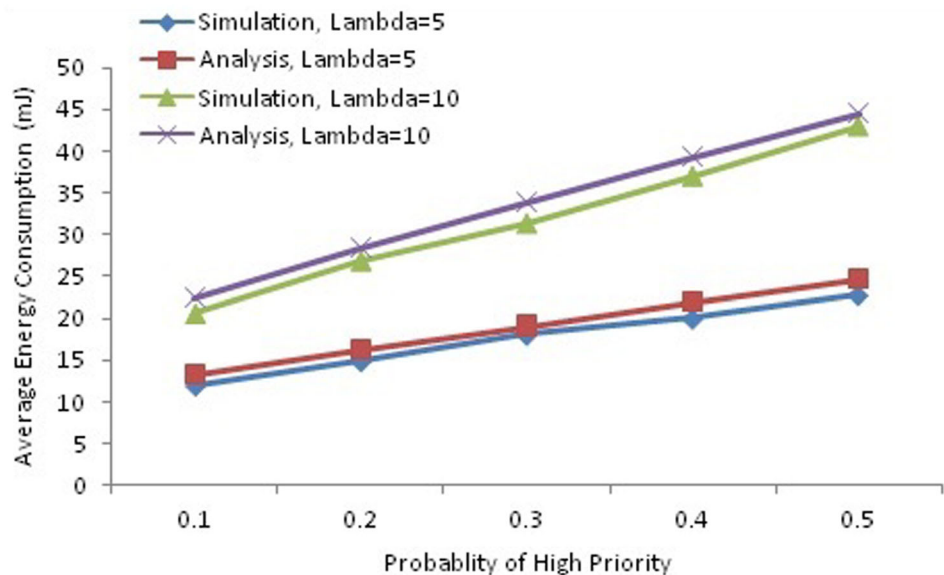
Arrival rate λ	Threshold N^*	Average Energy consumption (mJ)		% Increase in Energy Consumption
		NPM	PQM	
5	8	6.85	9.90	44.5
10	12	9.42	15.79	67.6

higher value of N is more when compared to that for a low value of N . Hence the average number of cycles per second is reduced when N increases.

Figure 6 shows the average energy consumption of a node for different values of N for PQM and NPM for mean arrival rate per node = 5 packets/s. From Fig. 6, it is inferred that, the average energy consumption using PQM is more when

compared to NPM because the number of cycles are more in PQM than NPM. As threshold increases, the average energy consumption per node decreases till some threshold and starts increasing after that threshold value and minimum energy is consumed for the optimal threshold. The optimal threshold value (N^*) using Eq. (9) for mean arrival rate per node of 5 packets/s is 8. From Fig. 6, it is also observed that the minimum energy is consumed for the optimal threshold value (N^*) = 8 for PQM.

Figure 7 shows the energy consumption savings (%) for different values of N . By assuming $N = 4$, $N^* = 8$, $N = 10$, and $N = 12$, and mean arrival rate per node = 5 packets/s, the energy consumption savings (%) is determined and it is found to be 56, 61, 60, and 59% respectively when compared to no threshold condition (i.e., $N = 1$). It is inferred that the (%) saving in energy consumption is maximum for the optimal threshold value (N^*) = 8.

Fig. 8 Probability of high priority packets versus average number of cycles**Fig. 9** Probability of high priority packets versus average energy consumption

Results are also obtained by varying the mean arrival rate per node and threshold number of packets by assuming $p = 0.1$ to determine the average energy consumption of a sensor node in a cluster and it is shown in Table 5. The average energy consumption is more for PQM when compared to NPM. It is also inferred that the (%) increase in energy consumption is high for PQM when compared to NPM.

Figures 8 and 9 implies that the average number of cycles per sec and average energy consumption of node increases for mean arrival rate per node = 5 packets/s and 10 packets/sec as the probability of high priority packets in node. This occurs as a result of increase in number of high priority packets which increases the transitions and hence energy consumption increases. Also, from Figs. 8 and 9, the average number of cycles per second and average energy consumption increases as the mean arrival rate per node in a cluster increases because when the arrival rate increases, the number of transitions increases thus resulting in increased number of cycles and energy consumption.

6 Conclusions and future work

This paper proposes a Modified Energy Minimization Scheme (MEMS) which reduces the average energy consumption of individual nodes in the cluster based heterogeneous sensor network using queue threshold based on M/D/1 Priority Queueing Model (PQM) in order to prolong the network lifetime of the HSN. The expression for the optimal value of queue threshold for which the node consumes minimum energy using PQM is also derived. Results show that the mean delay is highly reduced in PQM when compared to the NPM and the trade-off exist between the average energy consumption and mean delay is explored. We perform simulations and the results obtained show that the simulation results match with the analytical results thus validating the accuracy of the approach. The proposed PQM model is well suited for both delay sensitive as well as delay insensitive applications. In this work, the packets are transmitted from CH to BS directly since the H-sensors which acts as cluster head has more energy and longer transmission range. Though the CH has more energy supply, longer transmissions consumes more energy. Hence, the energy consumption at CH should be reduced because the failure of CH causes a cluster itself getting isolated from the BS. The energy consumed during the direct communication between the CH and BS should be considered to increase the lifetime of the CH. The savings in energy consumption can be achieved by introducing intra cluster routing which will be another interesting model of future extension.

References

1. Akyildiz, I.F., Su, W., Sankarasubramaniam, Y., Cayirci, E.: Wireless sensor networks: a survey. *Comput. Netw.* **38**(4), 393–422 (2002)
2. Huang, J., Hong, Y., Zhao, Z., Yuan, Y.: An energy-efficient multi-hop routing protocol based on grid clustering for wireless sensor networks. *Cluster Comput.* (2017)
3. Girod, L., Stathopoulos, T., Ramanathan, N., Elson, J., Estrin, D., Osterweil, E., Schoellhammer, T.: A system for simulation, emulation, and deployment of heterogeneous sensor networks. In: *Proceedings of the 2nd International Conference on Embedded Networked Sensor Systems—SenSys '04*, pp. 201–201 (2004)
4. Mhatre, V., Rosenberg, C.P., Kofman, D., et al.: A minimum cost heterogeneous sensor network with a lifetime constraint. *IEEE Trans. Mob. Comput.* **1**(1), 4–15 (2005)
5. Duarte-Melo, E., Liu, M.: Analysis of energy consumption and lifetime of heterogeneous wireless sensor networks. In: *Proceedings of the IEEE Globecom*, pp. 21–25 (2002)
6. Du, X., Guizani, M., Xiao, Y., Chen, H.-H.: Two tier secure routing protocol for heterogeneous sensor networks. *IEEE Trans. Wirel. Commun.* **6**(9), 3395–3401 (2007)
7. Jayaparvathy, R., Maheswar, R.: Energy minimization scheme for cluster based sensor networks. *Int. J. Recent Trends Eng. Technol.* **2**(6) (2009)
8. Jiang, F.C., Huang, D.C., Yang, C.T., Leu, F.Y.: Lifetime elongation for wireless sensor network using queue-based approaches. *J. Supercomput.* **59**(3), 1312–1335 (2012)
9. Maheswar, R.: Performance analysis of an energy optimization scheme for cluster based heterogeneous sensor networks, Anna University Thesis (2012)
10. Maheswar, R., Jayaparvathy, R.: Performance analysis using contention based queueing model for wireless sensor networks. In: *The International Congress for Global, Science and Technology*, pp. 59–59 (2010)
11. Maheswar, R., Jayaparvathy, R.: Performance analysis of cluster based sensor networks using N-policy M/G/1 queueing model. *Eur. J. Sci. Res.* **58**(2), 177–188 (2011)
12. Maheswar, R., Jayaparvathy, R.: Performance analysis of fault tolerant node in wireless sensor network. In: *Advances in Communication, Network, and Computing: Third International Conference, CNC 2012, Chennai, India (February 2012)*
13. Polastre, J., Hill, J., Culler, D.: Versatile low power media access for wireless sensor networks. In: *Proceedings of the 2nd International Conference on Embedded Networked Sensor Systems*, pp. 95–107 (2004)

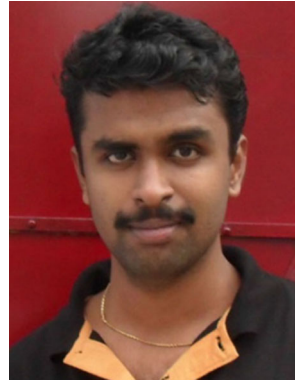


P. Jayarajan has completed his B.E. (EEE) from Madurai Kamaraj University in the year 2004, M.E. (Applied Electronics) from Anna University in the year 2008 and pursuing Ph.D. in the field of Wireless Sensor Network under Anna University. He has about 10 years of teaching experience and presently working as an Assistant Professor in the Electronics and Communication Engineering Department, Sri Krishna College of Technology, Coimbatore. He has published 10 papers at International Journals and Conferences. His research interest includes Wireless Sensor Network, Modelling and Simulation. He is a life member of ISTE.



R. Maheswar has completed his B.E. (ECE) from Madras University in the year 1999, M.E. (Applied Electronics) from Bharathiyar University in the year 2002 and Ph.D. in the field of Wireless Sensor Network from Anna University in the year 2012. He has about 15 years of teaching experience at various levels and presently working as a Professor in the Electronics and Communication Engineering Department, Sri Krishna College of Technology, Coimbatore. He has published

35 papers at International Journals and International Conferences. His research interest includes Wireless Sensor Network, Queueing theory and Performance Evaluation. He is a life member of ISTE.



G. R. Kanagachidambaresan received his Bachelor degree in Electrical and Electronics Engineering in 2010, Master's degree in Pervasive Computing Technologies in 2012 and Ph.D. in Information and Communication Engineering in 2017. He is currently an Associate Professor in Department of Computer Science and Engineering in Veltech Rangarajan Dr.Sagunthala R&D Institute of Science and Technology. His main research interest includes Body Sensor Network, Fault tolerant Wireless Network and IoT.

Battery Recovery Based Lifetime Enhancement (BRLE) Algorithm for Wireless Sensor Network

V. Mahima¹ · A. Chitra²

© Springer Science+Business Media, LLC 2017

Abstract Increasing the lifetime of the network and utilizing the resources to its maximum limit is the major issue in Wireless Sensor Network (WSN). The wireless sensor nodes in sensor network are powered using rechargeable batteries. However, providing energy to nodes in the remote environment is a major issue in WSN. Hence WSN needs a new energy efficient algorithm to enhance the network lifetime. In a sensor node, the transceiving module consumes more energy when compared to other modules. In this paper, a Battery Recovery based Lifetime Enhancement (BRLE) algorithm is discussed, which considers battery voltage curve for scheduling the transceiving module of the sensor nodes. The Markov model helps in determining the state of the sensor node as CH and CM based on battery recovery process. By scheduling the transceiving module based on the battery terminal voltage, recovery factor and distance between the nodes, the lifetime of the network is enhanced. Experimental results show that the algorithm outperforms the others by 1.38 times increased lifetime and 1.574 times increased throughput. The BRLE decreases the HOT SPOT and energy hole problem, avoiding loss in connectivity with the sink.

Keywords Wireless sensor network · Recovery effect · Energy management policy · Energy efficient · Hot spot · Voronoi

✉ V. Mahima
mahi.90may@gmail.com

A. Chitra
ctr.psg@gmail.com

¹ Electronics and Communication Engineering, Sri Krishna College of Technology, Kovaipudur, Coimbatore 641042, TAMIL NADU, India

² Department of Computer Applications, PSG College of Technology, Coimbatore, India

1 Introduction

The rapidly increasing applications of Wireless Sensor Network (WSN) have gained its importance in the field of modern research. Wireless Sensor Network (WSN) is a tiny embedded system distributed over a Region of Interest to serve the purpose of monitoring physical quantity. The resource constraint Wireless Sensor Network (WSN) has attracted a number of researchers in utilizing and managing the resources of the Sensor Nodes (SN). The need for remote monitoring and surveillance in anti-third environment has increased the growth of WSN. The sensor nodes consist of Sensing Unit, Processing Unit, Transceiving Unit and Powering unit. The sensor nodes must be small in size for the compatibility of the user. These nodes are deployed in remote environment, where battery replacement is tedious or impossible in nature [1–3]. So, higher the battery capacity greater will be the lifetime of the battery [4]. The constraints like size of the battery, chance to recharge and load given to the node motivates the designer to seek a new energy efficient algorithm for enhancing the lifetime of the network [5–9]. The clustered architecture of WSN has the capability to sense wide area and work for longer duration when compared to peer to peer and layered architecture. The Cluster Head (CH) in the clustered architecture acts as a full function device, which is capable of transmitting, receiving and transceiving the data. The CH receives data from its members in the cluster and transmits them to sink via other CHs [10, 11].

The concept of recovery effect is taken into consideration for designing the algorithm for energy management. The phenomenon of recovery effect occurs due to the fact that most of the energy is consumed from the edge of the battery, while some energy is deposited deeper inside the battery. When the battery has low discharge current or when it is left idle for certain duration, it gets a chance to recover the charge that is lost during high discharge cycles. This electro-chemical behavior of the battery replenishes the lost charge to certain level. The intermittent discharge of the battery during idle periods can help the battery to recover the lost charge to certain extent. The voltage level of the battery increases slightly during intermittent discharges. The efficient clustering mechanism based on recovery effect can improve the performance of the network by effectively loading the nodes. The current research in WSN focuses on effective utilization of resources to increase the lifetime of the network.

2 Related Works

The problem of maximum energy utilization from the battery is addressed through battery recovery effect. The continuous operation of sensor nodes causes the battery to deplete soon making the network unavailable for monitoring the event [4]. The intermittent drawing of energy from the battery can increase utilization of energy. The lifetime enhancement of the network is done based on optimal CH selection and optimal energy utilization from the battery [2, 3]. The battery runtime is examined based on battery recovery effect [5]. It is observed that beyond a saturation threshold, the contribution of idle time is less for battery recovery. The Markov chain framework is given to capture the battery recovery status. However the effective utilization of recovery effect is needed in clustering mechanism to improve the network lifetime. The battery recovery is done through stochastic markov chain framework concentrating battery degradation policy. The dynamic node lifetime estimation is done in [9] which is suitable for both static and dynamic loads. The factors such as battery type, self-discharge, charge cycles, discharge rate and temperature are analyzed. However, the method for complete utilization of

battery's energy is not discussed in this work. Many challenges on designing an energy efficient routing algorithm and utilizing the battery resource is discussed in paper [3, 5, 6]. The State of Charge (SoC) and Depth of Discharge of the battery are considered to enhance the lifetime of the node. The battery state and node lifetime is estimated in the papers [9–12] which deals about the state of charge under varying room temperature and operational conditions. The increase in lifetime is achieved through selecting optimal CH based on residual energy, distance [2, 6].

The higher probability of becoming a CH is given to the node with high residual energy in LEACH protocol [3, 5]. The LEACH-C algorithm [6] addresses partial unequal clustering. The LEACH-C algorithm lacks in addressing about the recovery effect and fails to effectively utilize the battery. The nodes are believed to be dead since it drains voltage, but it recovers after a particular duration and it becomes capable to transmit data for a shorter duration. The Battery friendly packet transmission algorithm addressed in [4] discusses about increase in lifetime based on the applications of sensor node. The battery is scheduled based on hard real time and soft real time applications. This work lacks in addressing about the energy hole problem of WSN [13–16]. In [14], a fuzzy logic based clustering approach is addressed with a technique of predicting remaining energy to prolong lifetime. The neural network training model is used to estimate Expected Energy Consumption. However the full battery utilization has not been addressed in the article. A Regional Aware Clustering with Isolated Nodes addressed in [6], concentrates on the nodes that are isolated from the cluster during cluster formation. As the isolated nodes consume more energy to communicate with the sink, the issue is addressed by considering residual energy and Regional Average Energy of all sensors in the cluster. The article [17–23] estimates the distance between nodes through RSSI parameter. In [19], the Battery Aware Routing Protocol is discussed in which the batteries are made to recover in an alternative manner to extend node lifetime. The routing is carried out through fully recovered nodes. This enhances the chance of recovery for all nodes in the cluster. The battery based model discussed in [24–27] provides node operation based on residual energy of the node and battery SoC. The sensor node lifetime primarily depends on the battery capacity. Effective utilization of battery resource is in need to enhance the individual node lifetime and network lifetime. The sensor nodes are elected as Cluster Head (CH) based on the residual energy of the node. The continuous energy utilization from battery does not utilize the charge available deep inside the battery. This problem can be addressed by effectively scheduling nodes with respect to recovery time of the battery. The following section discusses about the proposed Battery Recovery based Lifetime Enhancement algorithm.

3 Battery Recovery Based Lifetime Enhancement

The Battery Recovery based Lifetime Enhancement Algorithm (BRLE) considers recovery effect of the battery in the clustering scheme in order to improve the performance of the network. The nodes in the network are elected as CH based on the voltage status, discharge time and recovery time of the battery. The number of frames that can be sent by the node as a CH within prescribed voltage limit is calculated and node sending maximum number of frames (N_{frames}) is elected to be CH. The load given to the CH is maximum because it transmits and receives the data from other Cluster Members (CMs). The battery state is modeled with a piece wise linear equation. The Eq. 1 describes the battery model, in which

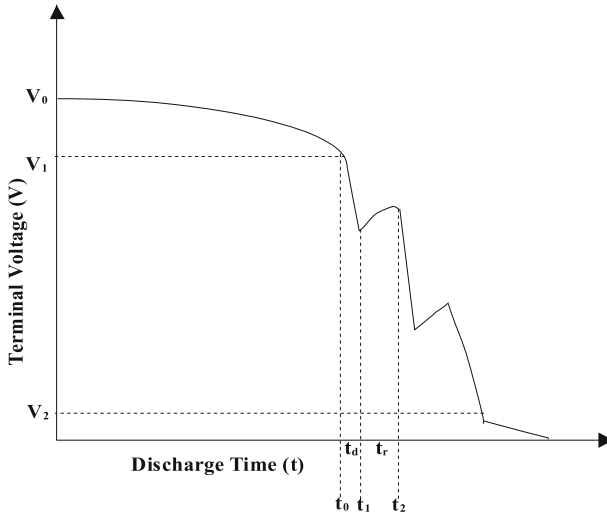


Fig. 1 Typical voltage curve of the Sensor node battery

the voltage limit V_1 and V_2 are set based on the battery voltage curve, in which V_1 refers the high voltage set limit and V_2 refers low voltage set limit of battery. The Fig. 1 describes the typical voltage curve, imposing the recovery effect of the battery [5]. The difference in t_2 to t_1 represents the time taken by the battery to recover the charge that is lost during high discharge or constant discharge currents.

Equation 1 illustrates the typical voltage curve of the battery with discharge and recovery phase. The voltage of the battery is increased after each recovery phase allowing the charges at the center part of the battery to migrate to the ends of the battery terminal.

$$F(V) = \begin{cases} mt & \text{for } t < t_1 \\ \frac{e^{-\beta^2(t_k-t_f)} - e^{-\beta^2(t_k-t_i)}}{\beta^2} & \text{for } t_1 < t < t_2 \\ 0 & \text{otherwise} \end{cases} \quad (1)$$

where $F(V)$ is voltage function of the battery, m slope of the curve, t time of discharge, V voltage value, β Diffusion parameter of the battery, t_k time for task k , t_i time when the load is turned on, t_f time when the load is turned off.

When the voltage level decreases below a threshold value 3.2 V and 2.2 V, the current drawn from the battery increases, in order to compensate the energy requirement of the node. This process further decreases the voltage level which makes the node to drain its energy soon. Equation 2 represents the energy dissipation in terms of voltage and current.

$$E = V_b \times I_b \times t_d \quad (2)$$

where V_b Battery end Voltage, I_b Current drawn from battery, t_d time required to transmit N_{frames} .

The decrease in voltage with respect to residual energy is derived from the battery voltage curve. The total number of frames that can be sent is derived through the radio energy model.

3.1 Battery Recovery Effect Modeling

The energy discharged by the battery during the n th slot of the whole lifetime of the battery is given in Eq. 3 as a function of diffusion parameter and time of operation.

$$F(T, n\delta, (n + 1)\delta, \beta) = \delta + \frac{\pi^2}{3\beta^2} \left[e^{-\beta^2(T-(n+1)\delta)} - e^{-\beta^2(T-n\delta)} \right] \tag{3}$$

where energy dissipated at n th time slot is denoted by $(n\delta, (n + 1)\delta)$, δ is the slot length, β battery diffusion rate. Let $\beta = \frac{2\pi\sqrt{D}}{W}$ the diffusion rate that depends on the distance- D between the electrode and width of the battery- W .

From the battery diffusion constant in Eq. 1 we obtain the charge discharged at n th time slot in Eq. 4. The charge dissipation is related with the load connected with the battery.

$$F(T, n\delta, (n + 1)\delta, \beta) = \delta + \frac{W^2}{12D} \left[e^{-\left[\frac{4\pi^2 D}{W^2}\right](T-(n+1)\delta)} - e^{-\left[\frac{4\pi^2 D}{W^2}\right](T-n\delta)} \right] \tag{4}$$

The battery recovery charge with respect to discharge rate, distance between electrodes, width and depth of discharge is given in Eq. 5 in which k is recovery slot.

$$\delta_n^k = \frac{I_n * W^2}{12D} \left[e^{-\frac{4\pi^2 D k \delta}{W^2}} - e^{-\frac{4\pi^2 D (k+1)\delta}{W^2}} \right] \tag{5}$$

From Eq. 5 the approximate recovery length t_r for n th time slot is given in Eq. 6 in which C is capacity of the battery.

$$t_r = \frac{W^2}{4\pi^2 D \delta} \log \frac{I_n W^2 \left(1 - e^{-\frac{4\pi^2 D \delta}{W^2}}\right)}{12DC} \tag{6}$$

4 Radio Energy Model

The energy dissipation of the nodes is realized with the radio model. The energy dissipated by the node for transmitting (E_{tx}) and receiving (E_{rx}) a bit of data is given in Eq. 7 and 8.

$$\begin{aligned} E_{tx}(k,d) &= E_{elec}k + E_{fs}kd^2; & d < d_0 \\ &= E_{elec}k + E_{mp}kd^4; & d > d_0 \end{aligned} \tag{7}$$

$$E_{rx}(k) = E_{elec}k \tag{8}$$

where k number of bits, d Distance, E_{elec} Energy dissipated per bit to run the transmitter or the receiver circuit, E_{fs} , E_{mp} Energy dissipated per bit ($\text{pJ}/(\text{bit}\cdot\text{m}^2)$) to run the transmit amplifier based on the distance between the transmitter and receiver.

Calculating (7) and (8) with (1) and (2) the voltage decay with respect to data transmission is observed. During recovery phase the node is transitioned to idle state. This allows the battery to recover for a duration t_r . After the recovery period, the nodes can participate in CH election.

Equation 9 represents the total number of frames sent to the sink by each node when it is selected as a CH before reaching the limit given in Eq. 4. The N_{frame} is calculated for the duration until the battery reaches the voltage limit V_1 . When the voltage limit of the battery decays below the voltage limit V_1 , the N_{frame} is calculated for the discharge time t_d .

$$N_{\text{frame}} = \frac{t_{CH}}{n \times t_{CM \text{ to } CH} + t_{CH \text{ to } BS}} \tag{9}$$

The nodes with reduced intra cluster distance and the nodes which are closer to the sink can send maximum number of frames. This methodology decreases the energy dissipation of the battery since the energy dissipation mainly depends on the distance of transmission of data. Selecting CH based on this approach increases the lifetime and total number of frames sent to the CH thereby increasing the throughput of the network. The sensor node is realized as a Finite State Machine (FSM) with CH, CM and Sleep/recover states.

5 Finite State Machine (FSM)

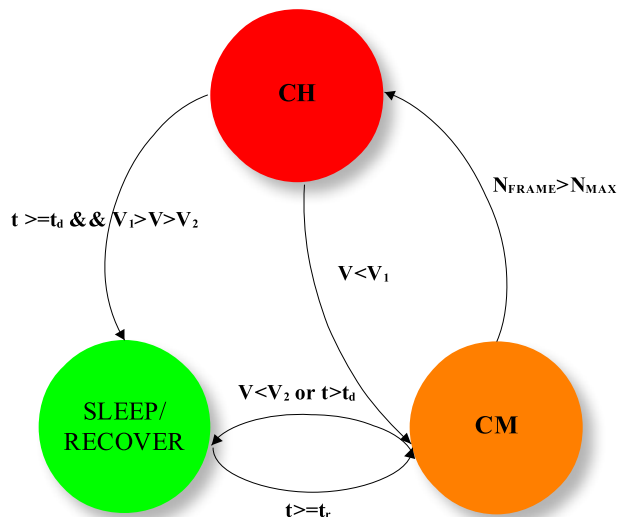
The operation of the node is modeled as FSM with three states (S_1, S_2, S_3). The S_1 represents the node operation as CH, S_2 represents the node operation as CM and S_3 represents the node operation as sleep and recover states. The state transition of the node is controlled by the value of voltage, discharge time and recovery time of the battery. The probability of transition from one state to other is predicted by the Markov model. The Markov model is the memory less model which works based on the current input to the system. The transition from one state to other mainly depends on the current value of voltage and distance and does not depend on the past interaction. The role of Sensor node is operated based on present situation and not on past and future events, hence the node is realized with markov model. Figure 2 describes the FSM representation of the sensor node.

Equation 10 and 11 denotes the next state transition in Markov chain. Probability of choosing x state to y state for n steps is given by

$$P_{xy} = P (P_n = y | P_0 = x) \tag{10}$$

The probability of single-step transition from x to k is given by

Fig. 2 Finite State Machine representation of the SN



$$P_{xk} = P(P_1 = q | P_0 = x) \tag{11}$$

Equation 12 and 13 represents the time homogenous transition from one state to other. The r step transition is chosen based on Eq. 12. For a time-homogeneous Markov chain

$$P_r(P_n = y) = \sum_{res} P_{ry} P_r(P_{n-1} = r) \tag{12}$$

Generalized probability of choosing r steps is

$$P_r(P_n = y) = \sum_{res} P_{ry} P_r(P_0 = r) \tag{13}$$

The probability P of transition from one state to other is represented by the matrix given in Eq. 14.

$$P = \begin{matrix} & \begin{matrix} S1 & S2 & S3 \end{matrix} \\ \begin{matrix} S1 \\ S2 \\ S3 \end{matrix} & \begin{pmatrix} P_{r11} & P_{r12} & P_{r13} \\ P_{r21} & P_{r22} & P_{r23} \\ P_{r31} & P_{r32} & P_{r33} \end{pmatrix} \end{matrix} \tag{14}$$

Figure 3 illustrates the proposed scheme of role selection for the Sensor Node. The CH selection is done based on the number of frames sent to sink. The Number of frames sent to the sink depends on the intra cluster distance, distance from node to the sink and their battery terminal voltages. The role of the sensor node (i.e.) as a CM, CH, and dead node is selected by the markov model and based on Voltage curve of the battery. The energy efficient battery recovery algorithm is described in Fig. 4. The candidates with

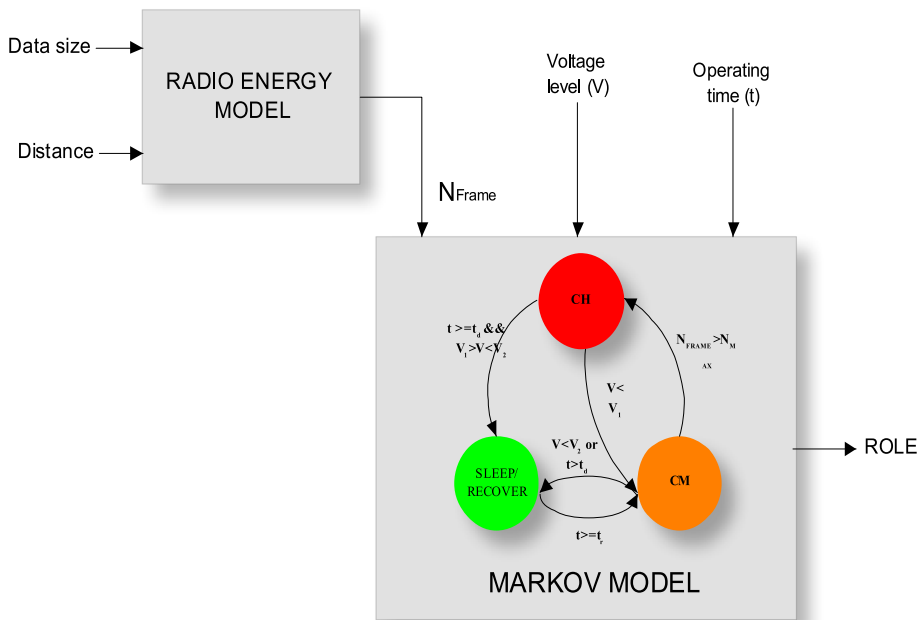


Fig. 3 Proposed scheme for role selection of sensor node

```

V1 :Voltage limit 1, V2 : Voltage limit 2, td : discharge time, tr: recovery time, d: distance, Vi: Voltage level of
individual node in Cluster, N: Number of nodes in Cluster, NFrame: Number of frames sent by node to CH.
Input: Voltage Vp, distance d, data size D
Output: Chance C
Function:
    Broadcast(Voltage point Vi, distance d);
    Send( data, destination);
Begin:
    while(Vi ∈ 1to N > V1)
        Compute total number of frames sent to destination (Nframe ∈ i node in the cluster)
        Select the eligible candidates (Nmax from Nframe)
    if1(Vi ∈ 1to N < V1)
        Compute total number of frames that can be sent within time td by all alive nodes within
        a cluster (Nframe ∈ i node in the cluster);
        Select the eligible candidate (Nmax from Nframe) ;
        if2(t > td)
            resign CH go to recovery;
            after recovery t > tr, participate as CM and go to if1;
            if3(Vi < V2)
                go to sleep;
            end if3
        end if2
    end if1
end while
End Begin

```

Fig. 4 Battery Recovery based Lifetime Enhancement (BRLE) algorithm

Table 1 Simulation preliminaries

Parameters	Values
Network size	100 × 100 m ²
Number of nodes	100
Base station location	(50, 125)
E_{elec}	50 nJ/bit
E_{fs}	10 pJ/bit-m ²
Initial energy	2 J
Probability of becoming a CH	0.1
Data size	2000 bytes
Header size	50 bytes
Wasmote battery parameters	
Battery voltage	4.2 V
On current	17 mA
Sleep current	30 μA
Capacity of battery	2300 mAh

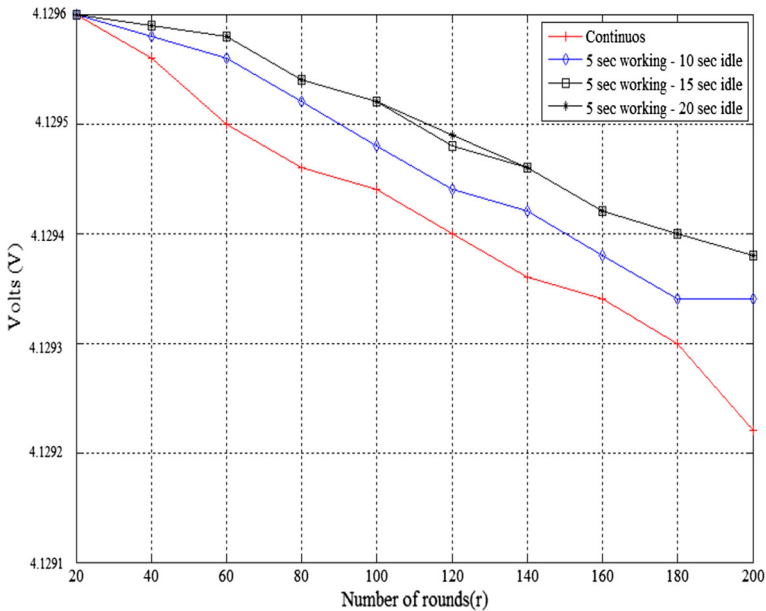


Fig. 5 Battery voltage curve with different idle times

Table 2 Recovery voltage (WASPMOTE)

S. No	t_d in s	t_r in s	V at the beginning of recovery (V)	V after recovery (V)
1	5	Continuous	4.12903	–
2	5	5	4.12903	4.129035
3	5	10	4.12903	4.129040
4	5	15	4.12903	4.129045
5	5	20	4.12903	4.129045

the voltage greater than V_1 are made eligible to participate in the election. The CH selection which happens before all nodes dissipate its voltage below V_1 is termed as High energy phase. In High energy phase, the number of frames that can be sent to the sink before reaching V_1 is calculated and the node capable to transmit high number of frames is elected as the CH. When all nodes in a cluster drain its voltage below V_1 , the corresponding cluster enters the recovery phase. The node is allowed to serve as the CH until the time t_d , above which the CH claims reelection and enters the recovery phase. The node is allowed to recover until time t_r as given in Eq. 1. The recovery time of the battery mainly depends on the State of Charge (SOC) of the battery β , which indicates the rate of recovery process. After recovery phase the node is allowed to participate in election.

Figure 4 illustrates proposed BRLE algorithm, where the voltage limits V_1 , V_2 and time limits t_d and t_r are selected from Eq. 1. The voltage value (V) of the node is enquired by sharing hello packet. The distance is estimated by the Received Signal Strength

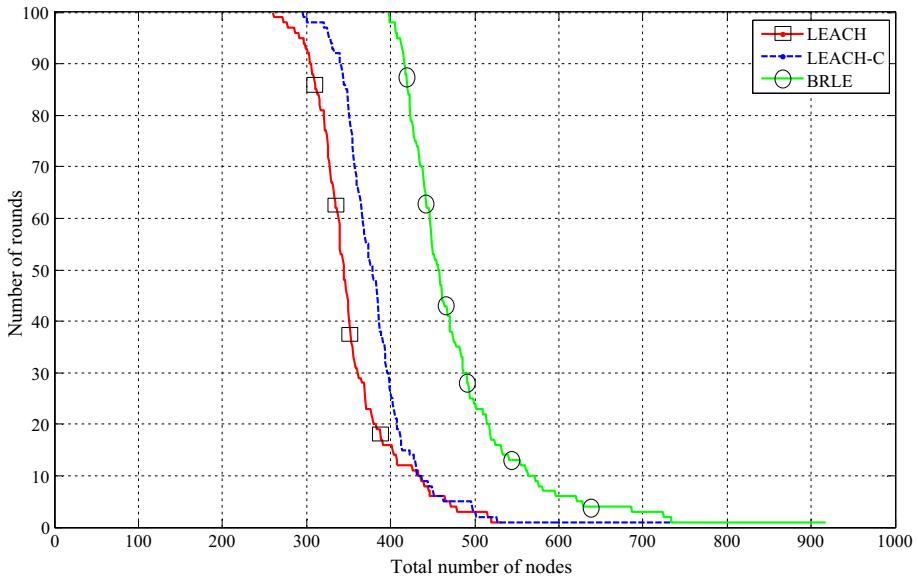


Fig. 6 Node survivability of LEACH, LEACH-C AND BRLE Algorithm

Indicator (RSSI). All nodes maintain a table regarding distance and Voltage value of the neighbor nodes.

6 Results and Discussions

The proposed BRLE algorithm is simulated with the parameters shown in Table 1. The proposed algorithm is simulated in MATLAB 7.0 and compared with LEACH and LEACH-C protocols. Following assumptions are made in the simulation

- All sensors are deployed in the ROI
- All nodes are energy constrained
- All nodes are either CH or Ordinary Node
- All nodes are static in nature
- All nodes are homogenous in nature

Figure 5 illustrates the typical recovery process of the Wasp mote (battery GE1653450—1S2P). The node is allowed to send data for 5 s and made idle for every 5 s. The distance between the sender and receiver is kept as 10 m. The pause time of the node after 20 s does not make significant change in the recovery process, stating all charges in battery are equally distributed across the battery. The recovery process completes by 15 s idle condition above which the idle time does not influence the rise in voltage. The discharge time and recovery time is modeled with Eq. 6. The recovery time for CH is modeled from Eq. 7 and 8 with battery drain characteristics Eq. 1. Table 2 illustrates the saturation in voltage (Fig. 1) after exceeding the recovery time as given in Eq. 6.

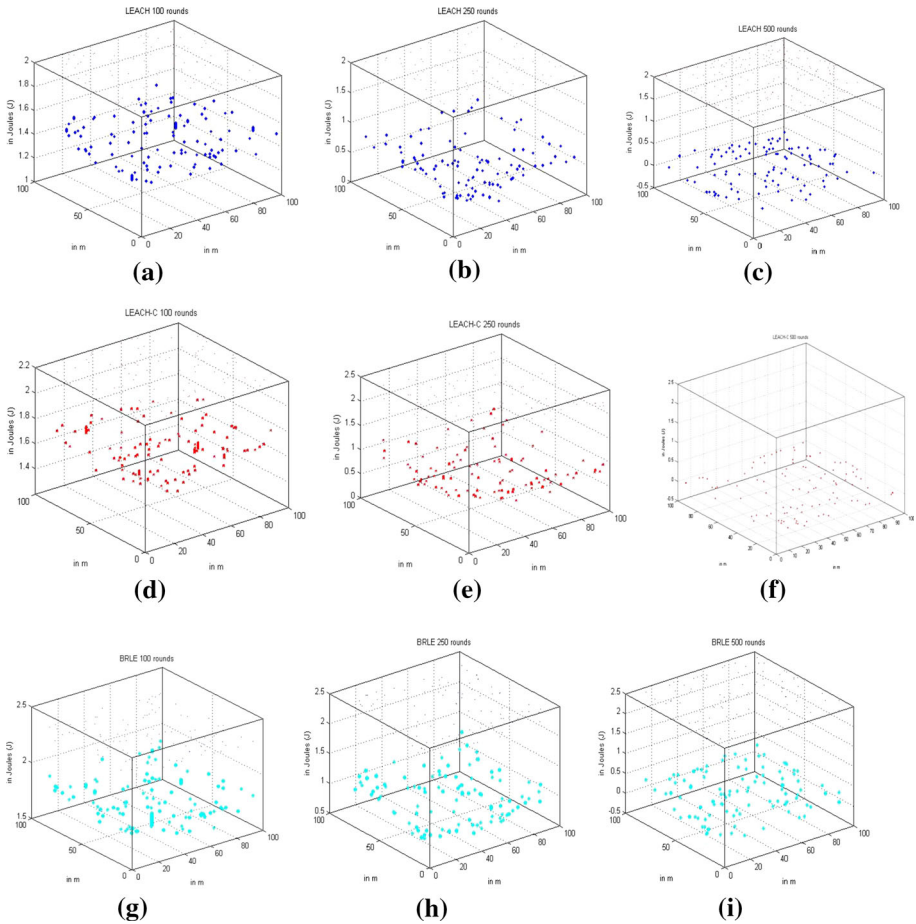


Fig. 7 a–i Residual energy of the nodes at 100, 250 and 500 rounds for LEACH, LEACH-C and BRLE algorithms

Figure 6 represents the node survivability of the three protocols; the BRLE outperforms the other protocols by 1.38 times. The proposed Fig. 6 elucidates the network lifetime of LEACH, LEACH-C and BRLE algorithms. The BRLE algorithm outperforms the LEACH by 1.432 times. The first node dies after 400 rounds in case of BRLE algorithm. But in case of LEACH and LEACH-C the node dies early in 248 and 297 rounds.

The BRLE algorithm shows improved throughput when compared with LEACH and LEACH-C algorithms. The BRLE shows 1.578 times improved throughput. The algorithm gives a better survivability when compared with other two protocols. The Energy distribution of nodes after 100, 250 and 500 rounds is depicted in Figure 7. The BRLE algorithm avoids energy holes showing equal load distribution. Figure 6 proves that the number of dead nodes in BRLE algorithm is less when compared to LEACH and LEACH-C algorithms. Figure 7a–c illustrates energy distribution of LEACH protocol where the nodes are loaded unevenly. Figure 7d–f denotes the energy distribution of LEACH-C

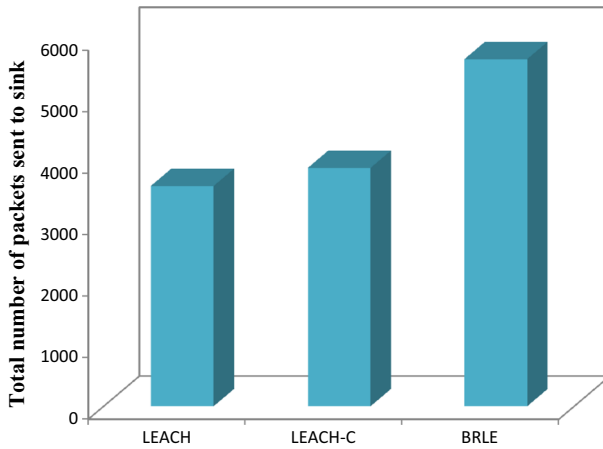


Fig. 8 Total number of packets sent to sink

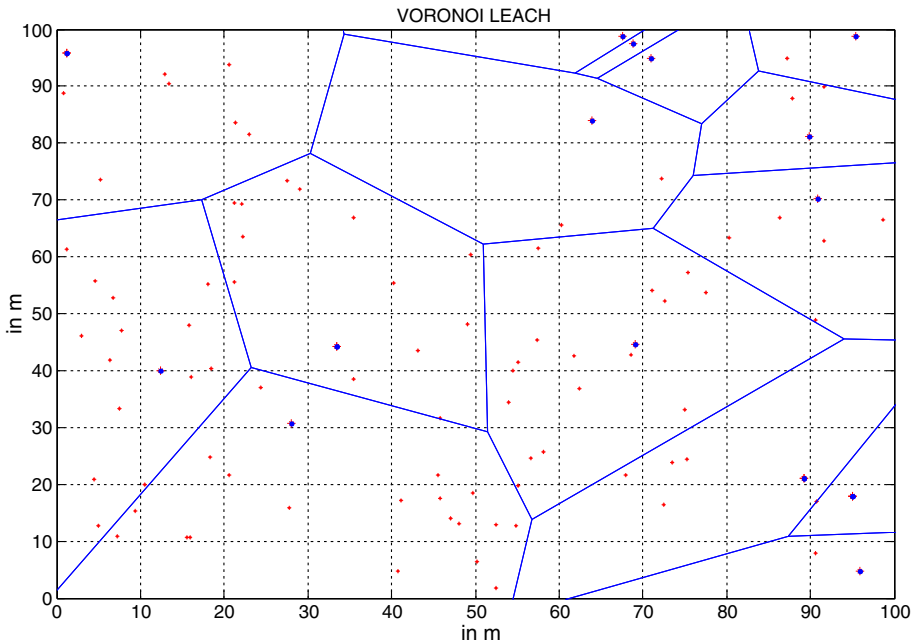


Fig. 9 VORONOI realization of LEACH protocol

protocol. Figure 7g–i denotes the energy distribution of proposed BRLE protocol. The nodes are evenly distributed in all cases (i.e.) in 100, 250 and 500 rounds.

Figure 8 illustrates the total number of packets communicated with the sink by three protocols. The BRLE outperforms the other two protocols by 1.574 times giving high throughput and increased lifetime to the network.